A machine learning approach targeting parameter estimation for plant functional type coexistence modeling using ELM-FATES (v2.0)

Lingcheng Li[1], Yilin Fang[2], Zhonghua Zheng[3], Mingjie Shi[1], Marcos Longo[4], Charles D. Koven[4], Jennifer A. Holm[4], Rosie A. Fisher[5], Nate G. McDowell[1,6], Jeffrey Chambers[4], L. Ruby Leung[1]

1. Atmospheric Sciences and Global Change Division, Pacific Northwest National Laboratory, Richland, WA, USA
2. Earth System and Science Division, Pacific Northwest National Laboratory, Richland, WA, USA
3. Department of Earth and Environmental Sciences, The University of Manchester, Manchester, UK
4. Climate and Ecosystem Sciences Division, Lawrence Berkeley National Laboratory, Berkeley, CA, USA
5. CICERO Center for International Climate and Environmental Research, Oslo, Norway
6. School of Biological Sciences, Washington State University, PO Box 644236, Pullman, WA, USA

Correspondence to: Lingcheng Li (lingcheng.li@pnnl.gov)

Highlight

- Machine learning based surrogate models were developed and used to optimize the selection of the trait parameters in ELM-FATES demographic vegetation model.
- Trait parameters selected by the surrogate models significantly improve the modeling of plant functional type coexistence and reduce model errors.
- This approach represents a repeatable method for identifying parameter values that satisfy fidelity against observations and coexistence between plant functional types in vegetation demography models across different ecosystems.

Abstract

Tropical forest dynamics play a crucial role in the global carbon, water, and energy cycles. However, realistically simulating the dynamics of competition and coexistence between different plant functional types (PFTs) in tropical forests remains a significant challenge. This study aims to improve the modeling of PFT coexistence in the Functionally Assembled Terrestrial Ecosystem Simulator (FATES), a vegetation demography model implemented in the Energy Exascale Earth System Model (E3SM) land model (ELM), ELM-FATES. Specifically, we explore (1) whether plant trait relationships established from field measurements can constrain ELM-FATES simulations; and (2) whether machine learning (ML) based surrogate models can emulate the complex ELM-FATES model and optimize parameter selections to improve PFT coexistence modeling. We conducted three ensembles of ELM-FATES experiments at a tropical forest site near Manaus, Brazil. By comparing the ensemble experiments without (Exp-CTR) and with (Exp-OBS) consideration of observed trait relationships, we found that accounting for these relationships slightly improves the simulations of water, energy, and carbon variables when compared to observations, but degrades the simulation of PFT coexistence. Using ML based surrogate models trained on Exp-CTR, we optimized the trait parameters in ELM-FATES, and conducted another ensemble of experiments (Exp-ML) with these optimized parameters. The proportion of PFT coexistence experiments significantly increased from 21% in Exp-CTR to 73% in Exp-ML. After filtering the experiments that allow for PFT coexistence to agree with observations (within 15% tolerance), 33% of the Exp-ML experiments were retained, which is a significant improvement compared to the 1.4% in Exp-CTR. Exp-ML also well reproduces the annual means and seasonal variations of water, energy and carbon fluxes, and the field inventory of above ground biomass. This study represents a reproducible method, which utilizes machine learning to identify parameter values that improve model fidelity against observations and PFT coexistence in vegetation demography models for diverse ecosystems. Our study also suggests the need for new mechanisms to enhance the robust simulation of coexisting plants in ELM-FATES, and has significant implications for modeling the response and feedbacks of ecosystem dynamics to climate change.

Plain Language Summary

Modeling tropical forest dynamics is crucial for understanding global carbon, water, and energy cycles under climate change. However, vegetation demographic models commonly struggle to realistically simulate the competition and coexistence of different plant functional types (PFTs). Our study explores whether plant trait measurements and machine learning surrogate models can improve plant coexistence modeling. We tested our approach using ELM-FATES at a tropical forest site. We found that using observed trait relationships did not improve PFT coexistence modeling. However, optimizing the trait parameters using machine learning-based surrogate models significantly improved PFT coexistence modeling and reduced model errors. We demonstrate the benefits of using machine learning to enhance PFT coexistence modeling, with important implications for modeling the response and feedbacks of ecosystem dynamics to climate change. Our study also highlights that new mechanisms are needed to robustly simulate coexisting plants in ELM-FATES.

1. Introduction

Tropical ecosystems feature the highest biodiversity on Earth, maintaining more than 75% of all known species (Mora et al., 2011; Mitchard, 2018). The dynamics of tropical forests are closely related to the regional and global carbon, energy and water cycles (Bonan, 2008; Piao et al., 2020). Vegetation is expected to face more water stress from vapor pressure deficit increase and soil moisture reduction with global warming (McDowell et al., 2020). Tree mortality rates are accelerating in some tropical regions due to rising atmospheric water stress (Bauman et al., 2022; Hubau et al., 2020; Zuleta et al., 2017). Tropical forests currently make an approximately neutral contribution to the global carbon cycle as a result of a large land-use source balanced by sinks in recovering and undisturbed forests, but they may become a carbon source in the future under the threat of climate change and human-induced disturbance (Mitchard, 2018; Gatti et al., 2021). Therefore, understanding and modeling tropical forest dynamics and related feedbacks have crucial implications for projecting future changes in the global climate system.

Dynamic global vegetation models (DGVMs) are the primary tools to simulate terrestrial ecosystem dynamics of plant functional type distribution, ecosystem composition and functioning, and ecosystem response to and recovery from disturbance (e.g., fire and wind damage) (Longo et al., 2019; Fisher et al., 2018; Foley et al., 1996; Sitch et al., 2003; Cao and Woodward, 1998; Berzaghi et al., 2019; McMahon et al., 2011). Conventional DGVMs represent plant communities using an area-averaged representation of plant functional types (PFTs) in each grid cell. Their relatively simple structures have the advantage of high computational efficiency for use in Earth system models (Fisher et al., 2018; Snell et al., 2014). However, these models do not capture many demographic processes. For example, plants of each represented PFT typically have identical

properties (e.g., tree size), which limits the capability of modeling ecosystem dynamics and functioning of canopy gap formation, PFT competition, and disturbance reactions (Feeley et al., 2007; Stark et al., 2012; Hurtt et al., 1998; Moorcroft, 2003; Brister et al., 2020). To address these limitations, researchers have developed new generation DGVMs called vegetation demographic models (VDMs), commonly including individual-based models and cohort-based models (Fisher et al., 2018). The individual-based models, also known as forest gap models, explicitly represent vegetation as individual plants and simulate their birth, growth, and death (Fyllas et al., 2014; Christoffersen et al., 2016; Sato et al., 2007; Jonard et al., 2020; Maréchaux and Chave, 2017). These models incorporate the stochasticity and heterogeneity of the plant light environment mechanistically and thereby can typically represent PFT competitive exclusion, succession, and coexistence. However, explicit simulations of individual plants with stochastic processes suffer a substantial computational penalty and limit applicability over large or global scales (Fisher et al., 2018). To capture sufficient ecosystem dynamics and maintain relatively high computational efficiency, "cohort-based" models have been proposed (Haverd et al., 2013; Medvigy et al., 2009; Ma et al., 2021; Moorcroft et al., 2001; Weng et al., 2015; Longo et al., 2019; Belda et al., 2022). In cohort-based approaches, individual plants are grouped together as "cohorts" based on their similar properties, including size, age, and PFT (Fisher et al., 2018). Many cohort-based models have been developed and widely used across regional to global scales. Examples of cohort-based models include the Ecosystem Demography model (ED) (Moorcroft et al., 2001), the Functionally Assembled Terrestrial Ecosystem Simulator (FATES) (Fisher et al., 2018, 2015), and the Geophysical Fluid Dynamics Laboratory (GFDL) Land Model 3 with the Perfect Plasticity Approximation (LM3-PPA) (Weng et al., 2015). In this study, we employ the FATES model, a widely used tool for modeling ecosystem dynamics in multiple ecosystems, including tropical

(Holm et al., 2020; Koven et al., 2020; Chitra-Tarak et al., 2021; Cheng et al., 2021), boreal (Lambert et al. 2022) and mixed-conifer forests (Buotte et al., 2021), and forest disturbance (Huang et al., 2020).

Despite ongoing applications, robust simulations of competition and coexistence in cohort-based VDMs remain a major challenge. In niche-based coexistence theory, coexisting species require both convergence in strategy to adapt to the surrounding environment ("environmental filtering") and divergence in strategy to ensure differentiation in resource requirements ("niche partitioning") (Kraft et al., 2008; Adler et al., 2013). These same constraints apply to coexisting PFTs as modeled by VDMs. Thus, on the one hand, VDMs need to include mechanisms that capture critical niche dimensions (e.g., spatial and temporal variation in light, water, and nutrients). For example, the multi-layer canopy structure in FATES provides vertical light resource differentiation. Another essential aspect is to assign reasonable plant functional traits (i.e., the parameters that define a given plant functional type) to satisfy environmental filtering, ensure niche partitioning, and consequently preserve PFT coexistence. Considering the relatively high computational cost of VDMs and the host land surface models, it is not feasible to directly apply global optimization methods such as Shuffled Complex Evolution (Duan et al., 1992) to calibrate trait-related parameters, because this could be time-consuming and computationally intensive (Rouholahnejad et al., 2012). Therefore, most previous studies use the filtered ensemble approach to select trait-related parameters involving several steps: 1) generate a parameter ensemble based on reference trait ranges or correlations, 2) conduct ensemble model simulations, and 3) filter the parameter ensemble by coexistence and other criteria (e.g., observation constraints). For example, Huang et al. (2020) applied FATES implemented in the Community Land Model (CLM; herein CLM-

138 FATES) with two tropical PFTs to study forest dynamics at tropical sites. They performed 70 one-
139 at-a-time experiments before obtaining one reasonable parameter set. Buottte et al. (2021) used
140 CLM-FATES to simulate forest dynamics of pine and incense cedar over the Sierra Nevada of
141 California, and their two stages of experiments (360 plus 72 runs) only yielded four sets of
142 parameters that met the given criteria. The filtered ensemble approach has low efficiency, which
143 hinders VDMs' application to modeling ecosystem dynamics under the changing climate. In
144 addition, trait relationships derived from field measurements are often used to infer parameter
145 selections when simulating coexistence. For example, Longo et al. (2020) used multiple trait
146 relationships derived from various datasets to guide parameter selection for different PFTs in the
147 ED-2.2 model simulations. However, whether the observed trait relationships can efficiently
148 improve PFT coexistence simulation in current VDMs is still unclear. Earlier studies using FATES
149 have also highlighted the importance of reproductive feedbacks in maintaining or prohibiting
150 coexistence (Fisher et al. 2010; Maréchaux and Chave 2017). But fundamentally, if PFTs have
151 highly contrasting reproductive output, the model tends towards competitive exclusion, so
152 discerning areas with at least approximately equal fitness is necessary. While representing a large
153 number of plant functional types may improve the likelihood of coexistence (Koven et al., 2020),
154 this comes at a considerable computational expense.
155
156 Machine learning (ML) has facilitated Earth science studies (Shen, 2018; Nearing et al., 2021; Zhu
157 et al., 2022; Pal et al., 2019; Jung et al., 2019), possibly providing a promising approach to improve
158 PFT coexistence modeling in VDMs. ML algorithms have been broadly and successfully
159 employed in recent decades. They can be used as standalone models to predict variables of interest
160 or integrated with process-based models to improve simulations (Xu and Liang, 2021; He et al.,

2022; Peatier et al., 2022). Among these applications, ML has shown advantages as a surrogate model for parameter optimization and sensitivity quantification, including its effectiveness and easy application, its ability to implicitly deal with complex nonlinear correlations and high dimensional data, and handle interactions between variables (Sit et al., 2020; Antoniadis et al., 2020; Tsai et al., 2021). One promising approach is to construct ML-based surrogate models using data from initial model simulations to emulate the relationship between inputs (i.e., model parameters) and model outputs (Wang et al., 2014). Then the computationally inexpensive surrogate model can be efficiently used for parameter optimization and sensitivity analysis. For example, Dagon et al. (2020) implemented artificial neural networks to emulate the satellite leaf area constrained version of CLM5 (Lawrence et al., 2019) and estimated optimal parameters to improve the global simulation of gross primary production and latent heat flux. Sawada (2020) developed an ML surrogate model to optimize the land surface model parameters and improve soil moisture and vegetation dynamics simulations. Watson-Parris et al. (2021) built a general tool to efficiently emulate Earth system models for uncertainty quantification and model calibration. Although employing ML based surrogate models to optimize the trait parameters and hence improve the vegetation dynamics modeling in VDMs is promising, this area of research remains under-explored.

This study aims to improve PFT coexistence modeling in VDMs. The cohort-based FATES implemented in the Energy Exascale Earth System Model (E3SM) land model (ELM; Golaz et al., 2019), i.e., ELM-FATES, is taken as our testbed. The ELM land model simulates surface energy fluxes, soil and canopy biophysics, hydrology, and soil biogeochemistry, whereas FATES simulates live vegetation processes, litter dynamics, and fire. We first examine whether trait

184 relationships constructed from field measurements can help improve ELM-FATES simulations.
185 Second, we explore whether ML based surrogate models can help optimize key trait parameters in
186 ELM-FATES to improve the simulation of PFTs coexistence. Our model experiments are
187 conducted for a tropical rainforest site located in Manaus, Brazil. This paper is organized as
188 follows. Section 2 describes ELM-FATES, summarizes the key functional trait-related parameters,
189 introduces the machine learning algorithms, and explains the overall experimental design. Results
190 are presented in Section 3, followed by Discussions and Conclusions in Section 4 and Section 5,
191 respectively.

2. Methodology

2.1 Study site and data

Our study site is located at kilometer 34 (K34) of the ZF2 road, Manaus, Brazil (latitude: -2.6091 S; longitude: -60.2093 W). The K34 site is an old-growth primary forest with minimal human disturbances (Holm et al., 2020). The annual precipitation is about 2252 mm, and the mean temperature is about 26.68 °C (https://ameriflux.lbl.gov/sites/siteinfo/BR-Ma2). The wet season is from November to May, and the dry season is from June to October (Fang et al., 2017). Hourly meteorological forcing (i.e., precipitation, air temperature, relative humidity, wind speed, surface pressure) at the K34 eddy covariance flux tower from 2002–2005 was obtained from the LBA-ECO CD-32 Flux Tower Network Data Compilation (Restrepo-Coupe et al., 2021). Observational reference datasets obtained from Holm et al. (2020) include gross primary production (GPP), evapotranspiration (ET), sensible heat flux (SH), Bowen ratio (BW, the ratio between sensible heat and latent heat), and inventory data-based aboveground biomass (AGB). The GPP, ET, SH, and BW observations are monthly climatological averages from 2000 to 2008 (Table S1). The AGB at this site is about 303 ± 2.3 Mg/ha. These observational data were used to evaluate the ELM-FATES simulations and constrain the ML surrogate models.

2.2 ELM-FATES and parameters

ELM-FATES is used as the model testbed. ELM is the land model of E3SM, which is the host land model of FATES (Golaz et al., 2019; Leung et al., 2020; Holm et al., 2020). FATES is a size- and age-structured vegetation model developed from the Community Land Model with ecosystem demography (CLM-ED) (Fisher et al., 2015; Koven et al., 2020). FATES includes two key structural components: ecosystem demography (ED; Moorcroft et al., 2001) and a modified

version of perfect plasticity approximation (PPA, Purves et al., 2008). FATES discretizes the simulated landscape into spatially implicit "*patches*" representing different disturbance histories of the ecosystem since the last disturbance. Within each patch, the hypothetical population of plants is grouped into "*cohorts*": a cohort consists of a population density of trees with similar size and the same plant functional type. Cohorts are organized, via the PPA concept, into canopy layers, and compete for light based on their canopy vertical positions (e.g., canopy layer vs. understory layer). The understory layer is formed when the canopy area becomes greater than the total ground area, and some fraction of each cohort is 'demoted' to the understory as a function of its height. The number of patches and cohorts varies depending on processes, including recruitment, growth, mortality, competition, and disturbance. The modified PPA probabilistically splits cohorts into discrete canopy and understory layers based on a function of their height (Strigul et al., 2008; Fisher et al., 2010). A detailed description of the FATES model can be found in its technical note (Zenodo, https://doi.org/10.5281/zenodo.3517272).

In this study, we configured two PFTs in ELM-FATES, i.e., early successional and late successional broadleaf evergreen tropical trees, which can represent a primary axis of variability in tropical forests (Huang et al., 2020; Reich, 2014; Díaz et al., 2016). There are tradeoffs between the plant traits of these two PFTs. Compared with the late successional PFT, the early successional PFT is more light-demanding and fast-growing, but with lower woody density, shorter leaf and root lifespans, and higher background mortality. To represent the drought impacts on forest dynamics, the early successional PFT is further assumed to be less drought resistant with shallower rooting depth and hence more easily affected by drought conditions (Oliveira et al., 2021). The corresponding tradeoffs and parameters between these two PFTs are shown in Figure 1 and Table

1.

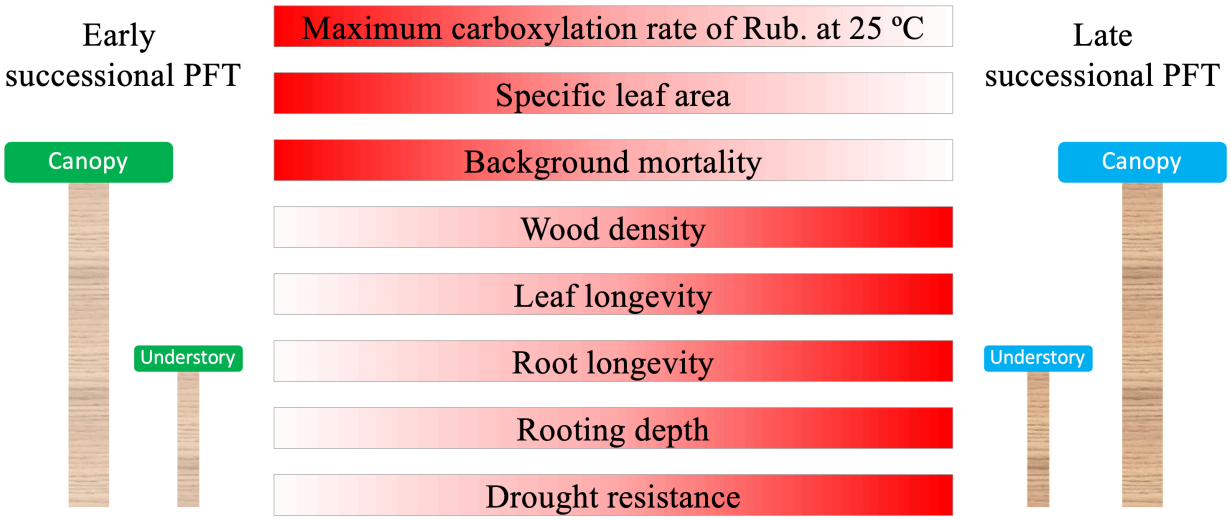

Figure 1. Schematic representation of tradeoffs between early and late successional PFTs. Dark red denotes a higher parameter value. The tradeoffs of the top five traits are used to constrain the parameter sampling.

Table 1 Summary of ELM-FATES trait parameters for two PFTs

Parameter type	Parameter name	Symbol	Unit	Early PFT	Late PFT	Range
Optimized parameter	Maximum carboxylation rate of Rub. at 25 ºC, canopy top	V_{cmax}	μmol $CO_2/m^2/s$	$V_{cmax,early} > V_{cmax,late}$		40–105
	Specific leaf area, canopy top	SLA	m^2/gC	$SLA_{early} > SLA_{late}$		0.005–0.04
	Background mortality rate	M_{bk}	1/yr	$M_{bk,early} > M_{bk,late}$		0.005–0.05
	Wood density	WD	g/cm^3	$WD_{early} < WD_{late}$		0.2–1.0
	Leaf longevity	L_{leaf}	year	$L_{leaf,early} < L_{leaf,late}$		0.2–3.0
	Maximum size of storage C pool, relative to the maximum size of leaf C pool	CR_{s2l}	—	same		0.8–1.5
Fixed parameter	Root longevity	L_{root}	year	0.9	2.6	—
	Fine rooting distribution profile parameter a	R_a	—	7	7	—
	Fine rooting distribution profile parameter b	R_b	—	2	0.4	—
	BTRAN threshold below which drought mortality begins.	M_{btran}	—	0.4	1.0E-06	—
	Soil water potential at full stomatal closure	$\psi_{closure}$	mm	–113000	–242000	—

*Parameter references (Huang et al., 2020; Koven et al., 2020; Longo et al., 2020; Holm et al., 2020; Cheng et al., 2021; Domingues et al., 2005; Chitra-Tarak et al., 2021; Buotte et al., 2021)

*R_a and R_b are parameters that determine the rooting depth and vertical distribution of fine roots.

*BTRAN is the plant water stress factor. BTRAN ∈ [0,1], 0 representing full water stress, 1 representing no water stress.

2.3 Machine learning algorithm

We built ML-based surrogate models to emulate ELM-FATES simulations. To represent the relationships between ELM-FATES parameters and simulations (e.g., AGB), we used eXtreme Gradient Boosting (XGBoost; Chen and Guestrin, 2016), a decision-tree-based ensemble machine learning algorithm. Ensemble learning techniques combine the predictions of multiple independent base models (e.g., decision trees) to produce more accurate predictions, with popular algorithms such as Random Forest (Breiman, 2001) and XGBoost. While Random Forest builds an ensemble of parallel trees using bagging and produces the final prediction by averaging the outputs of all individual trees, XGBoost sequentially trains a set of decision trees using boosting (Friedman, 2001), where each successive tree corrects the mistakes of its predecessors, and the final prediction is obtained by combining the predictions of all trees using a weighted sum. XGBoost not only handles complex nonlinear interactions and collinearity between different features, but also provides a parallel implementation that effectively solves a range of data science problems. It has been successfully applied in a variety of fields within Earth and Environmental Sciences, such as urban temperature emulation (Zheng et al., 2021b), wildfire burned area (Wang et al., 2021), and emissions prediction (Wang et al., 2022), flash flood risk assessment (Ma et al., 2021), and aerosol property estimation (Zheng et al., 2021a, c).

2.4 Experimental design

The experimental design flowchart is shown in Figure 2. Overall, we generated three ensembles of parameter values, i.e., Par-CTR, Par-OBS, and Par-ML, and conducted three ensembles of corresponding ELM-FATES experiments, i.e., Exp-CTR, Exp-OBS, and Exp-ML. Exp-CTR is the control experiment without being constrained by the observed trait relationships. Exp-OBS

considered the constraint of the observed trait relationships. The Par-ML was generated by machine learning surrogate models, which were trained based on Exp-CTR, and then used to conduct Exp-ML. The detailed experiment procedures are described below.

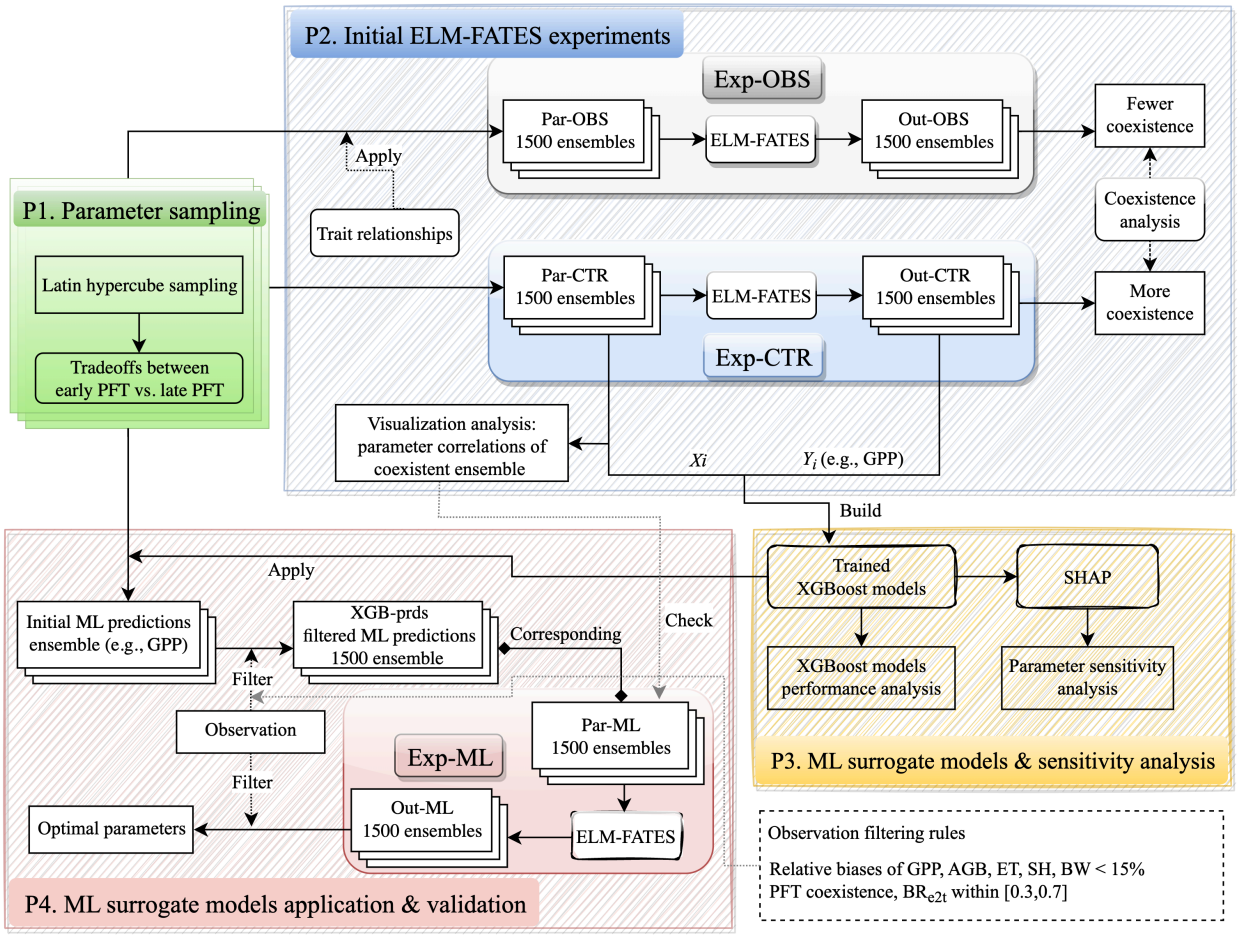

Figure 2. Overall flowchart of experimental design and associated analysis.

2.4.1 Procedure 1: Parameter sampling

The procedure "P1" in Fig. 2 is used to generate an ensemble of parameter values for each experiment ensemble, i.e., Exp-CTR, Exp-OBS, and Exp-ML. First, a number of initial parameter sets (e.g., 5000 sets) were generated using Latin Hypercube Sampling (LHS; Mckay et al., 2000). Second, the initial parameter sets were filtered by the trait tradeoffs between early and late successional PFTs (Figure 1). We repeatedly increased the number of initial parameter sets in the first step until 1500 parameter sets were obtained in the second step. Each ELM-FATES experiment starts from bare ground and runs for 350 years to reach an equilibrium state, by cycling the meteorological forcing during 2002–2005, and the last four years of the simulations were analyzed.

2.4.2 Procedure 2: Initial ELM-FATES experiments of Exp-CTR and Exp-OBS

To test whether plant trait relationships established from field measurements can improve the ELM-FATES simulations, we derived three trait relationships based on the tropical studies of Koven et al. (2020) and Longo et al. (2020). Using the digitized data from Figure 3 in Koven et al. (2020), background mortality M_{bk} (see table 1 for parameter definitions) can be empirically computed from V_{cmax},

$$M_{bk} = 0.0082 \times e^{(0.0153 \times V_{cmax})} \quad (1)$$

Based on the equations in Figure S18 of Longo et al. (2020), L_{leaf} and *WD* can be calculated via *SLA*-(see table 1 for parameter definitions),

$$L_{leaf} = 0.0001 \times SLA^{(-2.32)} \quad (2)$$

$$WD = -0.583 \times \ln(SLA) - 1.6754 \quad (3)$$

These trait relationships were used to generate parameters for Par-OBS.

Two initial sets of experiment ensembles, i.e., Exp-CTR and Exp-OBS (procedure "P2" in Figure 2), were conducted based on Par-CTR and Par-OBS, respectively. For Par-CTR, 1500 parameter sets were generated from the procedure "P1" based on the entire eleven parameters' space (i.e., $V_{cmax,early}$, $V_{cmax,late}$, SLA_{early}, SLA_{late}, $M_{bk,early}$, $M_{bk,late}$, WD_{early}, WD_{late}, $L_{leaf,early}$, $L_{leaf,late}$, CR_{s2l}). For Par-OBS, 1500 parameter sets were generated from the procedure "P1" but only based on five parameters' space (i.e., $V_{cmax,early}$, $V_{cmax,late}$, SLA_{early}, SLA_{late}, CR_{s2l}). The other six parameters ($M_{bk,early}$, $M_{bk,late}$, WD_{early}, WD_{late}, $L_{leaf,early}$, $L_{leaf,late}$,) in Par-OBS were calculated based on the traits relationships defined by Equations (1) ~ (3). Therefore, compared to Par-CTR, the parameters in Par-OBS are constrained by the observed trait relationships. The distributions of these two parameter sets are shown in Figure S1. V_{cmax}, *SLA,* and CR_{s2l} have similar distributions between Par-CTR and Par-OBS. Compared with Par-CTR, Par-OBS has a narrower distribution of M_{bk} but broader distributions of WD and L_{leaf}.

Exp-CTR and Exp-OBS each include 1500 350-year ELM-FATES simulations. We averaged the last four years of these simulations for analysis, i.e., simulation outputs: Out-CTR and Out-OBS, respectively. To quantify the PFT coexistence, we computed the biomass ratio between early successional PFT and the total biomass, denoted as BR_{e2t}. For brevity, we denote the ELM-FATES experiments with $BR_{e2t} \in [0.1, 0.9]$ as "coexistence", $BR_{e2t} \in [0.0, 0.1)$ as "late", $BR_{e2t} \in (0.9, 1.0]$ as "early". We calculated BR_{e2t} based on Out-CTR and Out-OBS, and then computed the fraction of coexistence experiments in each ensemble. As we will show in section 3.1, considering the observed trait relationships, Exp-OBS has a lower fraction of coexistence experiments. Therefore, only Exp-CTR was used for further ML-related analysis. We also

performed some analysis of Exp-CTR to explore whether the parameters of the coexistence experiments have correlations with each other (Section 3.2).

2.4.3 Procedure 3: ML surrogate models & sensitivity analysis

Based on Exp-CTR, we trained XGBoost models to emulate the ELM-FATES model behavior and analyzed the parameter sensitivity using SHAP (procedure "P3" in Figure 2). Sixteen variables were used as XGBoost model features, including 11 parameters in Par-CTR and 5 parameter differences between early and late successional PFTs. The corresponding ELM-FATES annual average outputs were used as XGBoost model targets. Specifically, six models were built, i.e., XGB_ET, XGB_SH, XGB_BW, XGB_GPP, XGB_AGB, XGB_BR for predicting ET, SH, BW, GPP, AGB, and BR_{e2t}, respectively. The ML models were trained and tested as described in Section 2.5, and subsequently utilized to perform the parameter sensitivity analysis (Section 2.5).

2.4.4 Procedure 4: ML surrogate models application & validation

The trained XGBoost models were then used to help select ELM-FATES parameters (procedure "P4" in Figure 2). First, initial parameter sets were generated from procedure "P1" based on the entire eleven parameters' space (Table 1, identical to the parameters' space used for the generation of Par-CTR). Second, these parameter sets and parameter differences were sent to six XGBoost surrogate models to predict ET, SH, BW, GPP, AGB, and BR_{e2t}. Third, the predictions were further filtered by two criteria: (1) compared to observations, the relative biases of the predicted ET, SH, BW, GPP, and AGB should be less than 15%; (2) the XGBoost model predicted BR_{e2t} should be within [0.3, 0.7], which corresponds to the range where the XGB-BR model exhibited relatively better performance (Figure 5). We repeated these three steps until we obtained 1500 sets of XGBoost model predictions that matched the criteria. Finally, we obtained 1500 sets of XGBoost model predictions and their corresponding 1500 sets of parameters (Par-ML). We also

checked whether the selected Par-ML could match the empirical relationships derived from the empirical analysis in procedure "P2" (see Sections 3.2 and 3.5 for details). Then, the 1500 sets of parameters in Par-ML were sent to ELM-FATES to conduct 350-year runs (i.e., Exp-ML). The last four years of the simulations were averaged (i.e., Out-ML) for further analysis. We then filtered Out-ML based on a relative bias of 15% or less compared to observations and PFT coexistence to identify the optimal experiments and corresponding parameters.

2.5 ML model development and SHAP analysis

The process of building each of the six ML surrogate models is described. Taking BR_{e2t}as an example, the 1500 pairs of sixteen features and the corresponding simulated BR_{e2t} were randomly split into two groups, 90% used for training and the remaining 10% used for testing. Given that the coexistence experiments only account for 20.6% in the simulations of Exp-CTR (Section 3.1), we used 90% of the data for training to ensure sufficient coexisting samples were included in the training process. Optimizing the hyperparameters of the XGBoost model is crucial for its performance. To achieve this, we employed the Bayesian optimization method during the training process (Snoek et al., 2012). In addition, to avoid overfitting during hyperparameter optimization, we utilized a five-fold cross-validation method (Feigl et al., 2021). The mean squared error was used as the objective function to achieve the optimal hyperparameters. The root mean squared error (RMSE) and R-squared (R^2) are used to quantify the overall model performance for the training and testing data prediction.

Based on the trained XGBoost models, we subsequently employed a game theoretic approach called SHapley Additive exPlanations (SHAP; Lundberg and Lee, 2017; Lundberg et al., 2018, 2020) to gain insights into the parameter sensitivity of ELM-FATES. SHAP assumes that features

(predictive variables) interact and collaborate in a prediction game, with each feature receiving a payout for its contributions. This approach provides a unified measure of feature importance to explain both individual samples and the entire dataset, which is distinct from intrinsic feature importance methods such as the feature importance in XGBoost (Lundberg and Lee, 2017). This approach has been widely used in various fields, including interpreting a digital soil mapping model (Padarian et al., 2020) and identifying the critical drivers of wildfires (Wang et al., 2021). In this study, we performed SHAP analysis for each XGBoost model and used the SHAP values as a proxy to quantify the relative importance of ELM-FATES parameters.

3. Results

3.1 Comparison between Exp-CTR and Exp-OBS

Constraining the input traits using the observed trait relationships yields slightly better ELM-FATES simulations of water, energy, and carbon variables (Figures 3a~3e). The distributions of the relative biases of ET, SH, BW, and GPP have similar ranges between the two sets of experiments (Figures 3a~3d). Compared with Exp-CTR, the 50th percentiles of relative biases of ET, SH, BW, and GPP for Exp-OBS (with constrained traits) are closer to zero, indicating Exp-OBS is slightly better than Exp-CTR. The distribution of simulated AGB for Exp-OBS is much narrower than Exp-CTR (Figure 3e), which could be due to the narrower distribution of M_{bk} (Figure S1).

Exp-CTR has a much higher fraction of PFT coexisting simulations than Exp-OBS (Figure 3f and Table S2). Overall, 70.6 % of experiments in Exp-CTR, and 94.5% of experiments in EXP-OBS have high simulated BR_{e2t} that is greater than 0.9. This indicates that both Par-CTR and especially Par-OBS favor the early successional PFT. As for the coexisting experiments with $BR_{e2t} \in [0.1, 0.9]$, Exp-CTR has about five times more coexisting experiments (20.6%) than Exp-OBS (4.1%). Further filtering the coexisting cases by observations (Table S1), only 21 experiments remain in Exp-CTR, and 6 experiments in Exp-OBS (Table S2). Even though Exp-OBS considered the observed trait relationships, it has fewer coexisting cases within the reasonable observation ranges than Exp-CTR. Therefore, Exp-OBS is not used in our remaining analysis.

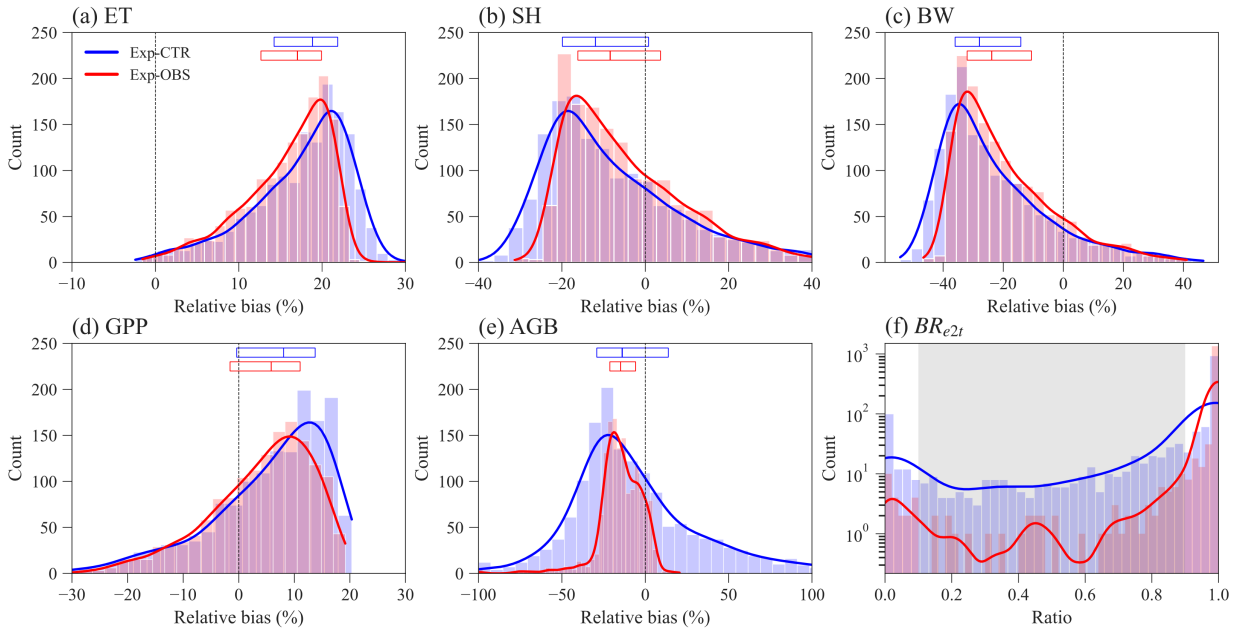

Figure 3. Distribution of ELM-FATES simulations for Exp-CTR and Exp-OBS. The y-axis in (f) is logarithmic. $Relative\ bias = \frac{simulation-observation}{observation} \times 100\ (\%)$. In (a)~(e), the top horizontal bars with three vertical lines denote the relative bias at the 25th, 50th, and 75th percentiles, respectively. The grey shaded area in (f) represents the coexistence biomass ratio between 0.1 and 0.9.

3.2 Parameter analysis of Exp-CTR

We also tested whether simple parameter correlations can be constructed to guide the simulation of PFTs coexistence. No simple parameter correlations can be built to distinguish the coexisting cases from the early and late cases in Exp-CTR (Figures 4, S2, and S3). Most parameter (or parameter difference) spaces show large overlaps between early, late, and coexisting cases (Figures S2 and S3). Notably, we empirically built three linear equations based on the boundaries in the parameter spaces for the coexisting cases (Figure 4). Coexisting cases are primarily located in spaces with $SLA_{late} > 0.35 \times SLA_{early} + 0.003$ (Figures 4a and 4d), $V_{cmax,diff} < -4800 \times SLA_{diff} + 100$ (Figures 4b and 4e), and $WD_{diff} > 55 \times SLA_{diff} - 1.3$ (Figures 4c and 4f),

where $V_{cmax,diff} = V_{cmax,early} - V_{cmax,late}$, and SLA_{diff} and WD_{diff} are defined likewise. Within these constrained parameter spaces, the percentage of coexisting cases increases from the original 20.6% (i.e., 309 out of 1500) to 32.6% (i.e., 304 out of 932). Therefore, these empirical correlations could help guide ELM-FATES parameter selection for coexisting PFTs. On the other hand, a dominant proportion (i.e., 67.4% (1–32.6%)) of experiments are still either early or late cases within the constrained parameter spaces and cannot robustly predict PFT coexistence. Moreover, despite further considering the observational constraints (black scatters in Figure 4; Table S2), the 21 experiments (2.3%, 21 out of 932) are still sparsely distributed in the parameters' space of the coexisting cases, so no simple correlations can be developed based on these simulations. Therefore, simple empirically built relationships between plant traits provide limited benefit to guiding ELM-FATES parameter selection for modeling PFTs coexistence while matching the observations. This finding provides additional motivation for the ML-based approaches.

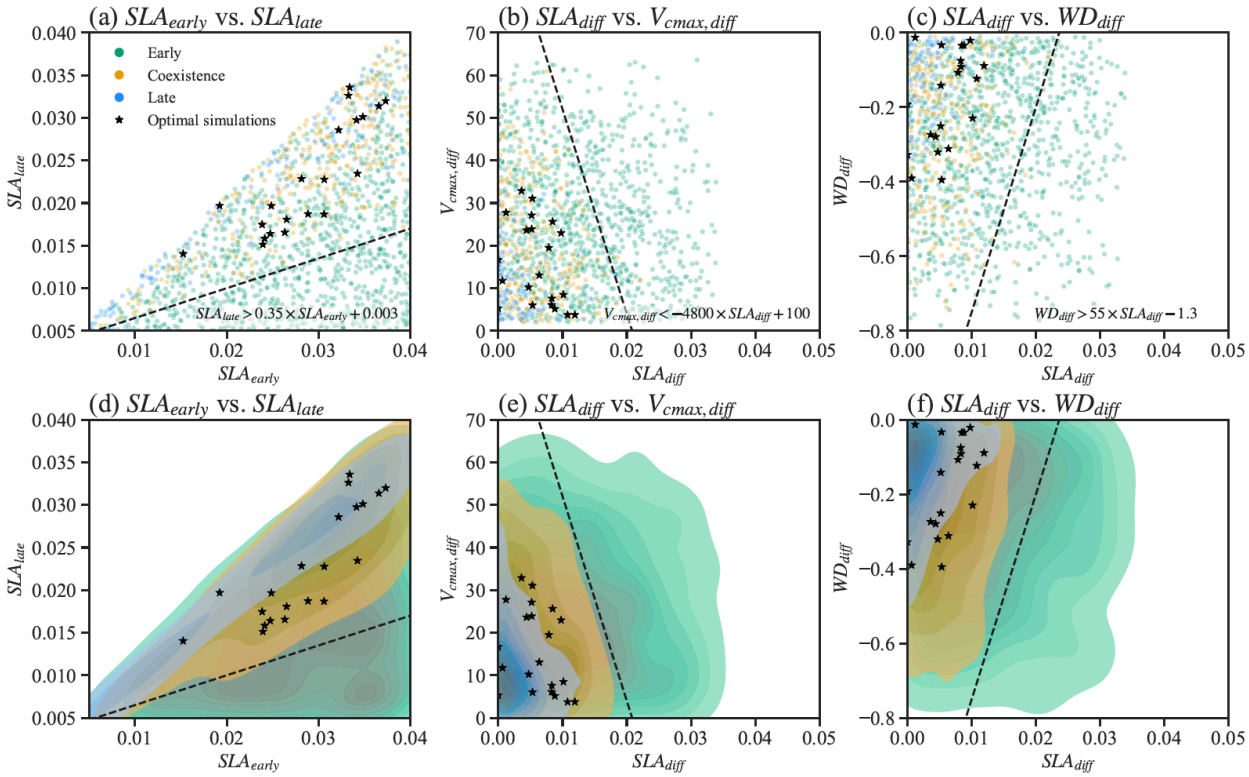

Figure 4. Relationships between selected parameters of Par-CTR. These parameters are presented in three groups, i.e., green color for the late cases with $BR_{e2t} \in [0.0,0.1)$, orange color for the coexisting cases with $BR_{e2t} \in [0.1,0.9]$, and blue color for the early cases with $BR_{e2t} \in (0.9,1.0]$. Black star represents coexistence cases further filtered by observational constraints. (d)~(f) are the corresponding kernel density estimate plots of the scatter plots (a)~(c). $V_{cmax,diff} = V_{cmax,early} - V_{cmax,late}$. SLA_{diff} and WD_{diff} are defined likewise.

3.3 XGBoost model performance

Overall, the XGBoost surrogate models show good performance in predicting ELM-FATES simulations (Figure 5). Based on Exp-CTR (i.e., Par-CTR and Out-CTR), six XGBoost models were trained. In training, the RMSEs for the six models are zero or nearly zero, and R^2s are close to one. In the testing, four XGBoost models (i.e., XGB_ET, XGB_SH, XGB_BW, XGB_GPP)

still show good performance with small RMSE and large R^2 (>0.95). XGB_AGB shows a little degradation with R^2 of 0.88. The performance of XGB_BR also shows degradation with R^2 decreasing from 1.0 in training to 0.75 in testing. XGB_BR cannot well predict the ELM-FATES simulated BR_{e2t} of 0 or 1 when only one PFT survives. This indicates that PFT competition processes in ELM-FATES, which determine BR_{e2t} and AGB, are highly nonlinear and difficult to emulate even using a state-of-the-art machine learning algorithm.

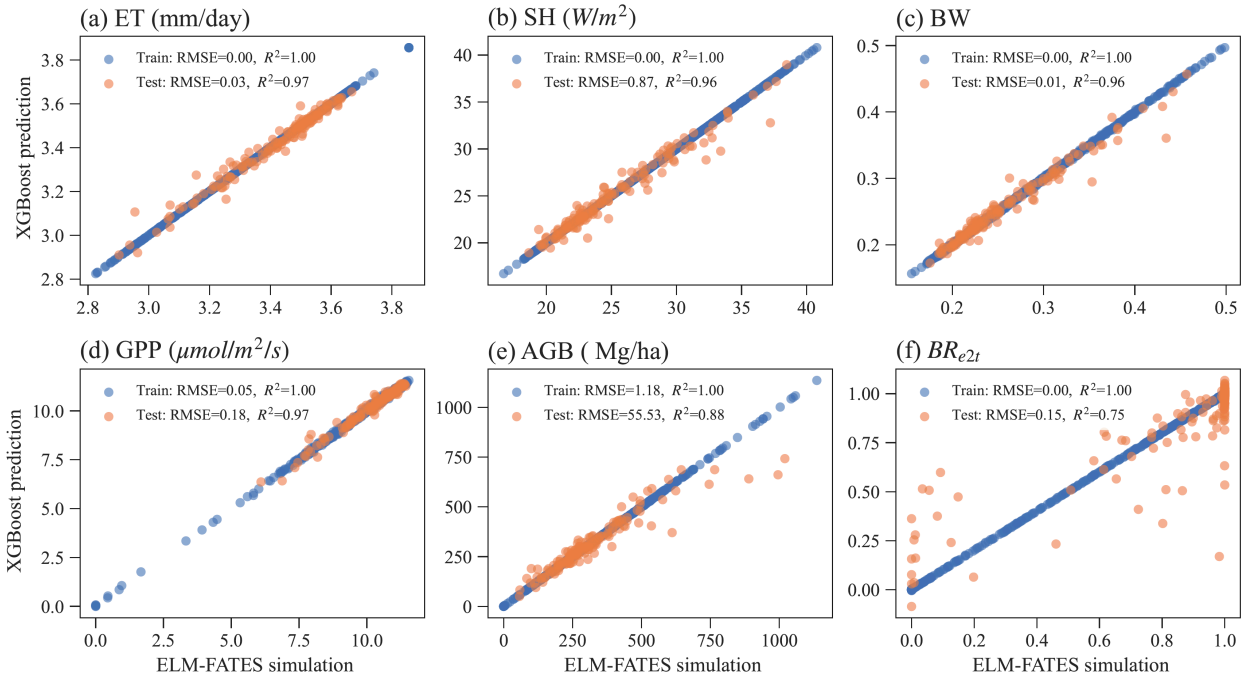

Figure 5. The performance of XGBoost surrogate models in the training and testing for predicting (a) ET, (b) SH, (c) BW, (d) GPP, (e) AGB, and (f) BR_{e2t}.

3.4 SHAP parameter importance analysis

Figure 6 shows the feature importance, including parameters and parameter differences, for different XGBoost models. Features (on the y-axis) with a higher mean absolute SHAP value (on the x-axis) denote a larger contribution to the XGBoost model prediction. The number of most

important features is different for predicting ET, SH, BW, and GPP compared with predicting AGB and BR_{e2t}.

For the XGBoost models that predict ET, SH, BW, and GPP, the top three features have the largest SHAP values compared to the rest (Figures 6a~5d). Notably, these top three features are the same and correspond to the early successional PFT, i.e., $V_{cmax,early}$, SLA_{early}, and $L_{leaf,early}$. Most ELM-FATES experiments in Exp-CTR used as the training samples for the XGBoost models are early cases. Therefore, the parameters of early successional PFT have dominant contributions in the XGBoost model predictions of overall grid-level fluxes. These three parameters are positively correlated with ET and GPP and negatively correlated with SH and BW (red vs. blue bars in Figures 6a~d; Figure S4 for more details), reflecting the fundamental carbon metabolism of the typically dominant early successional plant.

For the XGBoost surrogate models of AGB and BR_{e2t}, more than eight features have large SHAP values (Figures 6e and 6f). Both early and late successional PFT parameters contribute to predicting the two variables. Compared with the predictions of ET, SH, BW, and GPP with only three major features, predicting AGB and BR_{e2t} is relatively more complex. This is because AGB and particularly BR_{e2t} are closely related to the PFT competition process in which both the early and late PFT traits are crucial. Especially for BR_{e2t}, the most important features are the parameter difference between the early and late successional PFTs. For example, SLA_{diff} is positively correlated to BR_{e2t}. Therefore, to have coexisting PFTs with $BR_{e2t} \in [0.1,0.9]$, the SLA of two PFTs should neither be too large nor too small.

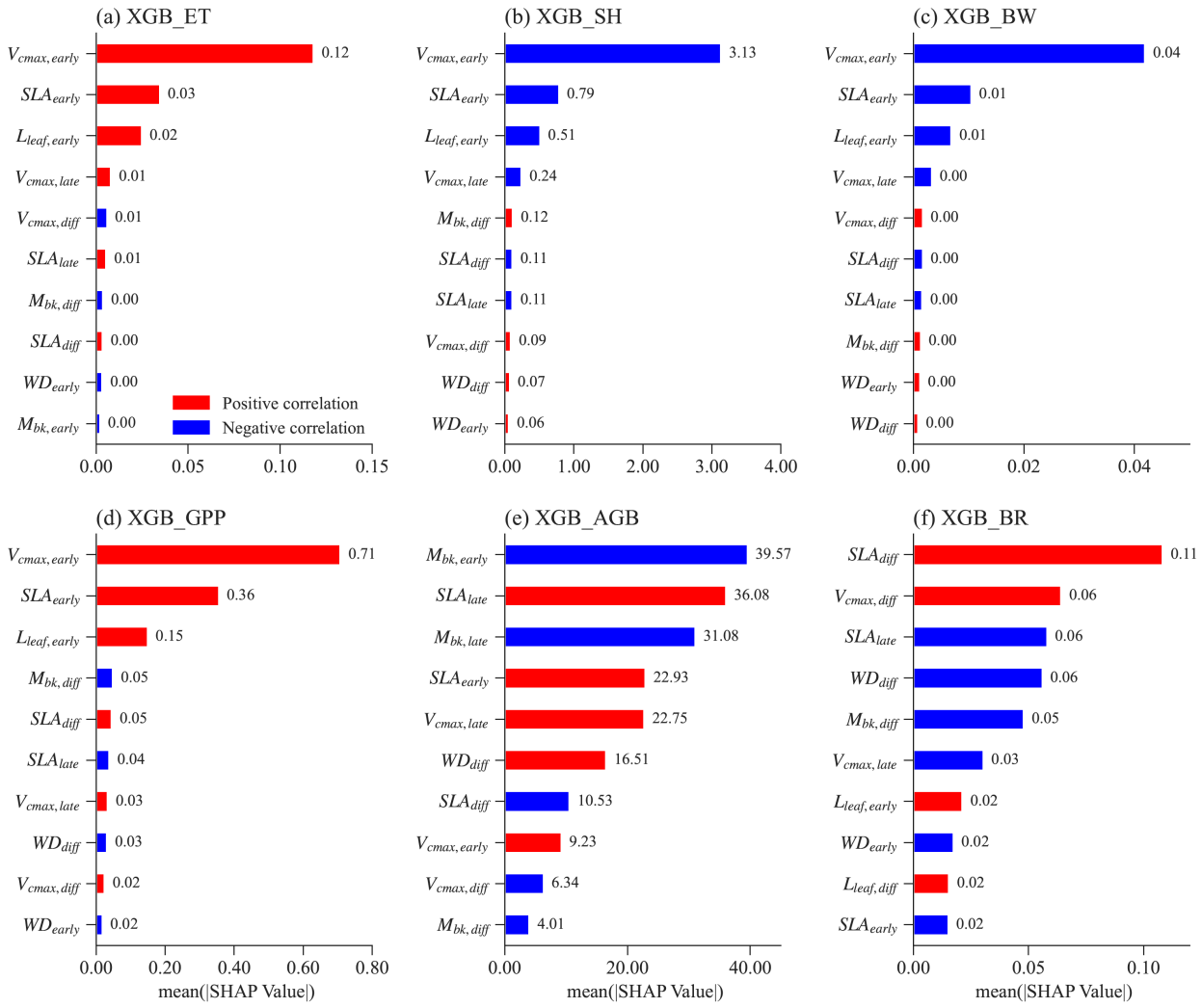

Figure 6. Mean absolute SHAP values for different XGBoost surrogate models for the top ten most important features. Absolute SHAP values are sorted in decreasing order from top to bottom. For each feature (y-axis) in each XGBoost model, the Spearman correlation coefficient is calculated between the feature values and the corresponding SHAP values (Figure S4). The red color means that a given feature is positively correlated with the predicting variable, whereas blue denotes a negative correlation.

3.5 XGBoost model parameter selection

Using the XGBoost surrogate models, the Par-ML was selected, including 1500 sets of parameters and the corresponding parameter differences between the early and late successional PFTs (Section 2.4, procedure "P4" in Figure 2). We examined whether Par-ML matches the empirical relationships shown in Figure 4 (Section 3.2), i.e., $SLA_{late} > 0.35 \times SLA_{early} + 0.003$, $V_{cmax,diff} < -4800 \times SLA_{diff} + 100$, and $WD_{diff} > 55 \times SLA_{diff} - 1.3$. In total, 99.1% (1486 out of 1500) of parameter sets are consistent with the empirical relationships, indicating the XGBoost models implicitly learned these simple relationships.

The parameter distributions of Par-ML show different patterns from the early/late parameters of Par-CTR (green vs. blue regions in Figure 7), but there are large overlaps between the coexistence parameters of Par-CTR and Par-ML (orange vs. green regions, e.g., the third column in Figure 7). This indicates that the XGBoost surrogate models learned to select parameters around the parameters' space of the coexisting cases. Par-ML also tends to have a smaller parameter difference between the early and late successional PFTs in terms of SLA_{diff} and $V_{cmax,diff}$. However, Par-ML also shows different patterns from the coexisting parameters of Par-CTR, probably because the XGBoost selected parameters were also constrained by multiple observations and implicitly considered parameter tradeoffs. For example, the $V_{cmax,early}$ and $V_{cmax,late}$ of Par-ML are located in narrower ranges than the coexisting parameters of Par-CTR (first two columns in Figure 6).

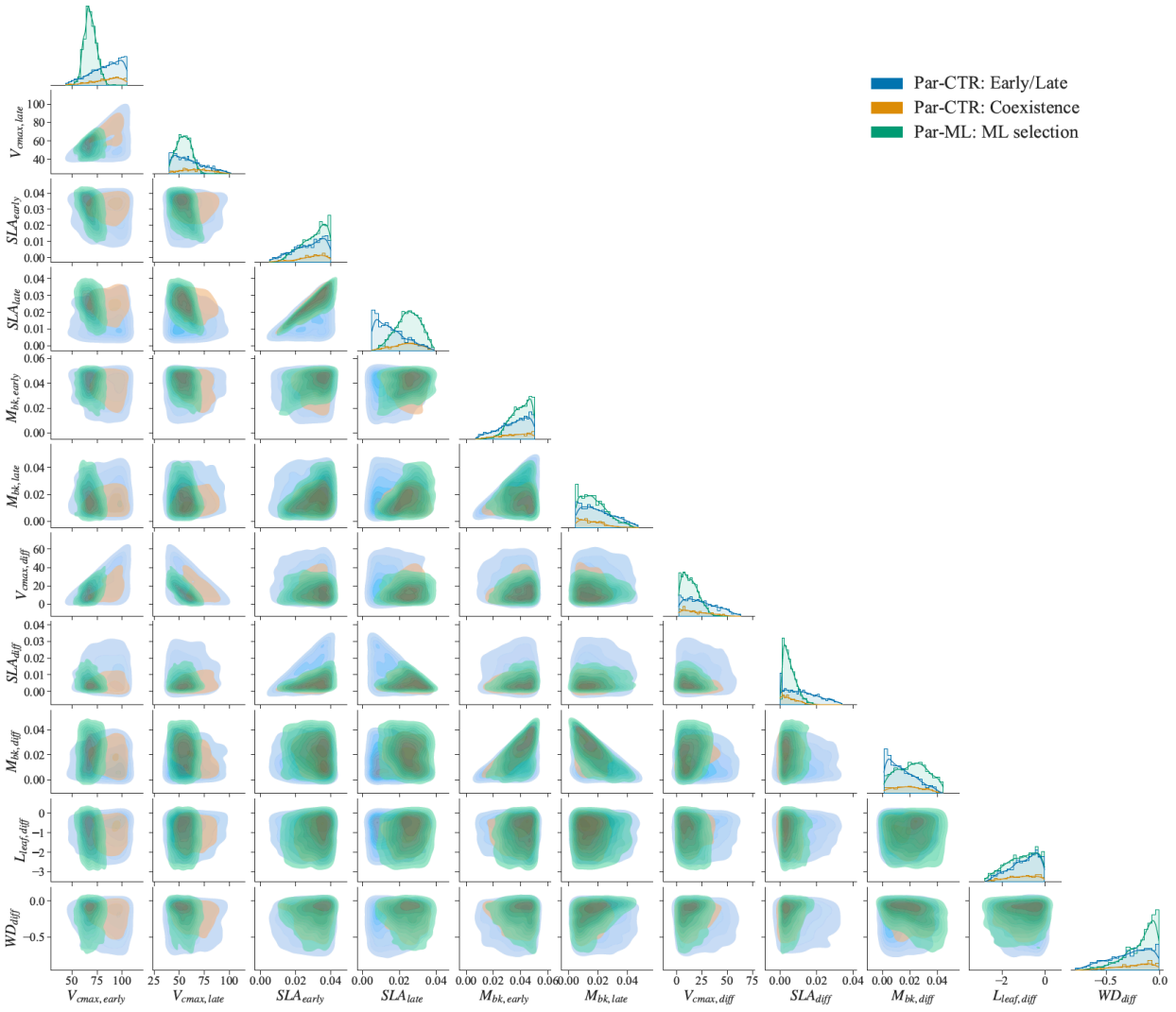

Figure 7. Comparison of parameter or parameter difference in Par-CTR vs. Par-ML for eleven features. The diagonal plots represent each parameter's distribution, and the rest of the subplots are kernel density estimate plots. There are three groups, i.e., blue for the early/late cases of Par-CTR, orange for the coexisting cases of Par-CTR, and green for Par-ML selected by XGBoost models.

3.6 Validation of ML selected parameters

ELM-FATES simulations of Exp-ML based on the ensemble parameters of Par-ML selected by the XGBoost surrogate models can better capture the observations and have more coexisting cases than Exp-CTR (Figure 8). The median values of simulated variables for Exp-ML are closer to observations with relative biases closer to zero than Exp-CTR (Figure 8a, blue vs. green boxes). The Exp-ML simulated variables also have more concentrated distributions than Exp-CTR. Compared to the skewed distribution of BR_{e2t} in Exp-CTR with a large proportion of early cases, Exp-ML has a more normally distributed BR_{e2t} (Figure 8b). Specifically, Exp-ML has about 3.6 times more coexisting cases than Exp-CTR, i.e., 73.1% (1097 out of 1500) in Exp-ML vs. 20.6% (309 out of 1500) in Exp-CTR (Table S3). After being further constrained by observation (Table S3), one-third of the experiments (i.e., 495 out of 1500) in Exp-ML remain, and this ratio is 23.6 times more than 1.4% (21 out of 1500) in Exp-CTR.

The XGBoost surrogate model predicted variables also match well with those simulated using ELM-FATES in Exp-ML (Figure 8, orange vs. green boxes), indicating the overall reasonable accuracy for the XGBoost model predictions. Compared to the ELM-FATES results using Par-ML, the XGBoost models show better performance for ET, SH, BW, and GPP, but relatively degraded performance for AGB and BR_{e2t} (Figure S5). It is consistent with the performance of the XGBoost models' training and testing results (in Section 3.3).

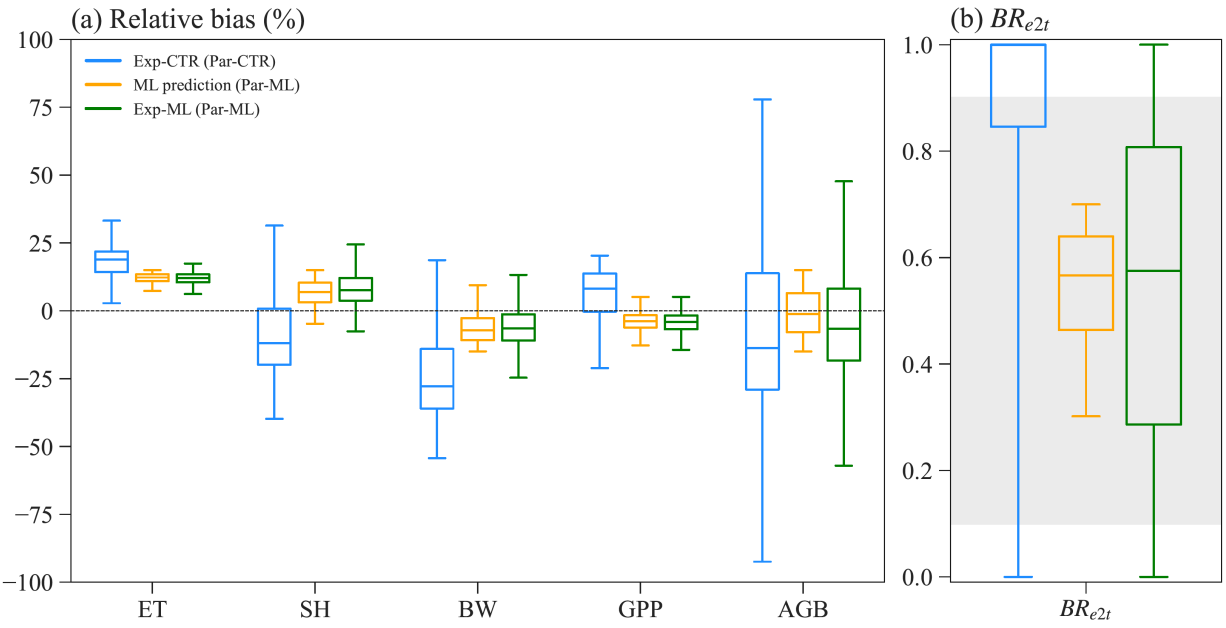

Figure 8. Comparison between the ELM-FATES simulations for Exp-CTR and Exp-ML. (a) Relative bias for simulated ET, SH, BW, GPP, and AGB. (b) Simulated BR_{e2t}. ML prediction represents the selected XGBoost model predictions after filtering with observation and biomass ratio (i.e., the XGB_prds, procedure "P4" in Figure 2).

3.7 Parameter tradeoff for coexistence experiments

Parameters of the early and late successional PFTs show tradeoffs for the coexisting experiments. Large relative differences in SLA, V_{cmax}, and WD (more negative) favor the early successional PFT, while large relative differences in M_{bk} and L_{leaf} favor the late successional PFT. Therefore, in Exp-CTR, compared to the early and late cases, the coexisting cases have intermediate relative differences in SLA, V_{cmax}, WD, M_{bk}, and L_{leaf} (dashed boxes in Figure 9). The coexisting cases in Exp-ML have similar patterns with intermediate relative differences in SLA, V_{cmax} and L_{leaf} compared to the early and late cases (solid boxes in Figure 9). However, M_{bk} and especially WD show the largest relative difference for the coexisting cases compared to the early and late cases

in Exp-ML. These two parameters still show a tradeoff in determining coexisting PFTs, because larger WD favors the early PFT while larger M_{bk} favors the late PFT.

In Exp-ML, the parameter spaces of the coexisting cases show large overlaps with the early/late cases (Figure S6). There are no simple correlations between these parameters to distinguish the coexisting cases from the early and late cases (also see Section 3.2). Although WD_{diff} of the coexisting cases still overlap with the early/late cases, when WD_{diff} is less than roughly –0.4 (g/cm^3), only coexisting cases exist (Figure S6). Nevertheless, this rule (i.e., $WD_{diff} <- 0.4$) alone cannot ensure PFT coexistence (see Figure 7).

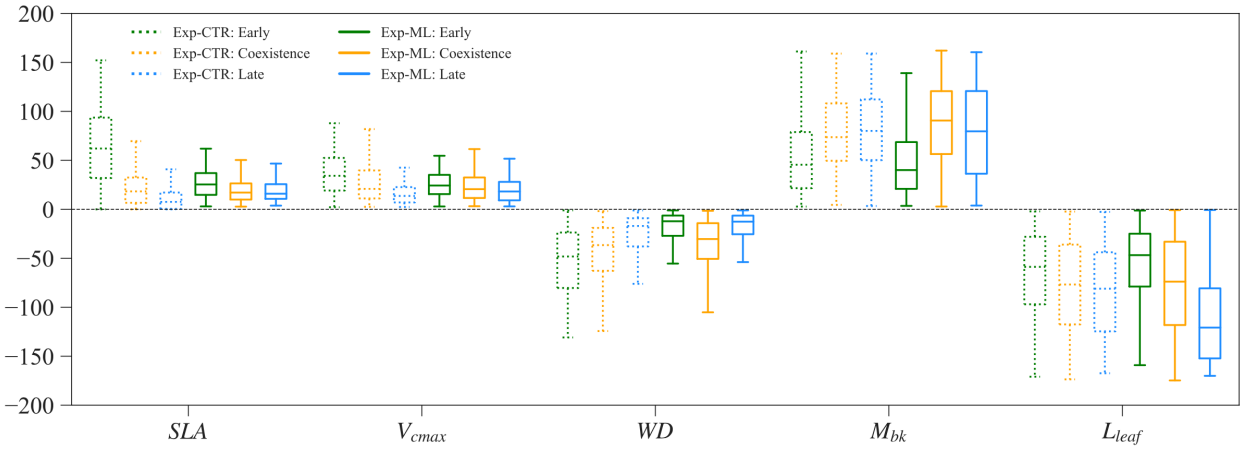

Figure 9. Parameter relative difference (%) between early successional PFT and late successional PFT for Exp-CTR (box with dash line) and Exp-ML (box with solid line). Parameter relative difference is calculated as, taking SLA as an example, $\frac{SLA_{early}-SLA_{late}}{(SLA_{early}+SLA_{late})/2} \times 100$ (%).

3.8 Seasonal variation comparison

Figure 10 shows the seasonal variations of ET, SH, BW, and GPP for observations and simulations of the finally selected 495 experiments in Exp-ML with good model performance (Table S3). Overall, the simulated ET shows a similar seasonal variation to ET observation (Figure 10a), with relatively small ET in the wet season (November–May), high ET in the dry season (June–October), and ET peaks in August. However, compared to the observations, ELM-FATES overestimates ET, especially during the wet season. The simulated SH also shows a similar seasonal variation with the SH observation except in March. ELM-FATES overestimated SH from January to May but underestimated SH from September to December (Figure 10b). Due to the discrepancy between simulated ET and SH, the model underestimates BW from September to December (Figure 10c). The simulated GPP has minor seasonal variability compared to the observed GPP. ELM-FATES overestimates GPP from June–August in the dry season, but underestimates GPP over October–December. The lower GPP over June–August indicates that plants may be relatively water-stressed or energy limited during these months. However, the large ET observation over the same period implies that this site is unlikely water limited or strongly energy limited. The ELM-FATES simulations also display little water stress year-round (Figure S7). Therefore, there are likely elements of the seasonal cycle (e.g., phenological responses of photosynthetic capacity) that are not yet captured here. Additionally, tower estimates of GPP may also have large uncertainties.

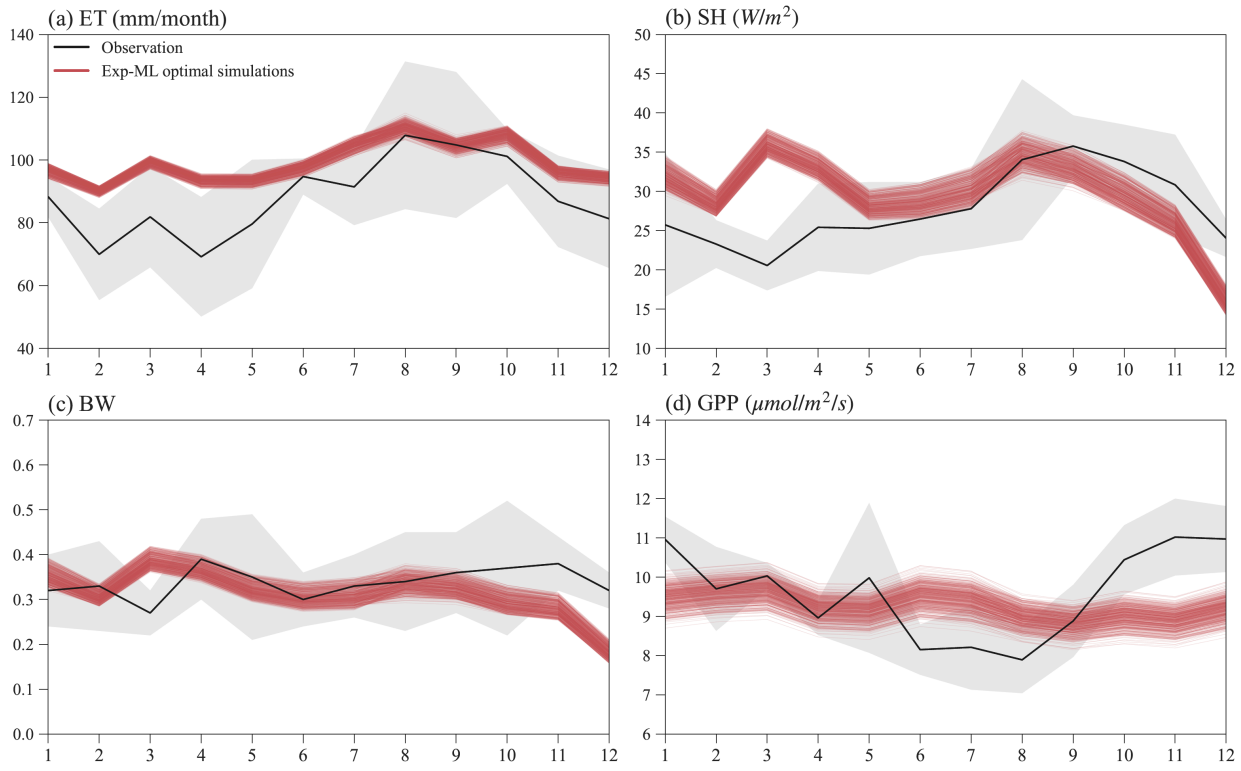

Figure 10. Mean monthly observations and selected optimal ELM-FATES simulations in Exp-ML for (a) ET, (b) SH, (c) BW, and (d) GPP. Each red line represents one experiment simulation (four-year simulation average). The black curves are monthly climatologic averages from 2000 to 2008, and the grey shaded area represents the interannual variabilities (i.e., $mean \pm standard\ devation$).

4. Discussion

4.1 Limited guidance of observed trait relationships for PFT coexistence modeling in FATES

We found degraded PFT coexistence in ELM-FATES simulation when observed trait relationships are considered. More specifically, constrained by observed trait relationships, Exp-OBS has fewer coexisting cases than Exp-CTR which does not consider the observed trait relationships. The observed trait relationships were derived from site measurements in the species-rich tropical ecosystem where plant coexistence commonly happens (Kraft et al., 2008), which is expected to enhance the PFT coexistence simulations. This inconsistency could be due to several possible reasons. First, ELM-FATES is a typical "trait filtering" model (Fisher et al., 2018), and the realistic simulation of PFT dynamics largely depends on the fidelity with which trait tradeoff surfaces are prescribed in the model (Scheiter et al., 2012). Implicit representation of trait tradeoff in the current ELM-FATES model may not be well balanced, which may differ from the observed trait relationships that lead to coexistence in the real world (at least for the ecosystem at our study site). In particular, there may be correlated tradeoffs that are measured (e.g., with below ground processes, Chitra-Tarak et al. 2021) but not represented in the model. A second reason could be the mismatch between different spatial scales. The observed trait relationships are derived from field measurements across tropical forests over a large region with diverse species and climate, e.g., the relationship in equation (1) is for plant species in Panama. In contrast, ELM-FATES simulations were conducted at the K34 site scale with specific species composition. Therefore, the large-scale trait relationships may not reflect the small-scale trait relationships. Wright et al. (2005) showed that trait relationships fitted for individual sites varied considerably. Third, the observed trait relationships are based on simplified equations, which may not be able to comprehensively reflect PFT coexistence. For example, although equation (2) derived from Longo et al. (2020) can

596 reflect the negative relationship between SLA and L_{leaf}, the R^2 of this equation is about 0.49,
597 which may not be accurate enough to represent trait relationships. Additionally, these equations
598 (1)~(3) do not consider the uncertainty of traits covariance. In Koven et al. (2020), the uncertainties
599 between trait covariance were considered when sampling parameters for FATES experiments.
600 Furthermore, machine learning models can also be employed to extract the relationships between
601 plant traits, which can then be incorporated into ELM-FATES and evaluated in future studies.
602
603 **4.2 Advantages of ML surrogate models on improving PFT coexistence modeling**
604 ELM-FATES simulations driven by parameters selected using the XGBoost models essentially
605 improved PFT coexistence and better captured observations. Compared to the initial Exp-CTR,
606 which was used to train the XGBoost models, the proportion of coexisting PFTs in Exp-ML
607 reaches 73.1%, 3.6 times more than 20.6% in Exp-CTR. Further filtering the coexistence
608 experiments by observations, Exp-ML still has 33.0% of experiments left with good model
609 performance, 23.6 times that of 1.4% of experiments in Exp-CTR with good performance. Our
610 ML-based approach also outperforms the empirical correlations built in Section 3.2, which only
611 yields 32.5% of coexistence experiments and this reduces to 2.3% of experiments if further
612 constrained by observation. The large proportion of optimal experiments selected by our ML
613 approach also outperforms previous studies using direct filtering approaches. Buotte et al. (2021)
614 conducted two stages of experiments to select optimal parameters for CLM-FATES modeling with
615 two conifer species; only 0.3% (1 out of 360) of the cases met the given criteria in the first stage
616 experiments, which increased to 5.5% in the second stage experiments. Huang et al. (2020)
617 conducted CLM-FATES modeling with two tropical PFTs at the Tapajós National Forest sites;
618 only one parameter set out of seventy (about 1.4%) was selected with reasonable fractions of two

PFTs and minor errors compared to observations. In addition, the parameter selection procedures of these two studies require some degree of subjective decision making and expert knowledge. On the other hand, our ML-based approach takes a more objective procedure, and little expert knowledge is required except for the initial determination of the parameter reference ranges. Importantly, we believe this approach can be repeatable as, e.g., model developments lead to changes between the parameter values and model predictions of forest structure and function, and can be used to define constrained ensemble values that will allow assessment of confidence in model predictions. Even though simulating the coexistence of different plants may not be a big concern for individual-based VDMs, e.g., LPJmL-FIT (Sakschewski et al., 2015, 2016) and TROLL (Maréchaux and Chave, 2017), our approach also could be applied to the selection of key parameters that regulate vegetation dynamics in these models.

Our study also reproduced the observations satisfactorily. Holm et al. (2020) conducted the ELM-FATES simulation with only one PFT considered at the same K34 site. Our study yields better or similar performance in the magnitude of AGB, and the magnitude and seasonal variation of GPP, ET, SH, and BW (Table 2 and Figure 3 in Holm et al. 2020 vs. Figures 8 and 10 in this study). It should also be noted that the overestimation of simulated energy fluxes (latent heat and SH) from January to May could be associated with the energy-related processes (e.g., energy partition, surface albedo) in ELM-FATES. Other potential reasons could be related to the uncertainties in atmospheric forcing and the common issue of incomplete energy budget closure at eddy covariance towers (Wilson et al., 2002; Foken, 2008; Rocha et al., 2009).

Compared to the predictions of GPP, ET, SH, and BW simulated by ELM-FATES, the XGBoost surrogate models show slightly degraded performance in predicting the simulated BR_{e2t} and AGB (Figures 5 and S5). Three parameters ($V_{cmax,early}$, SLA_{early}, and $L_{leaf,early}$) mainly control the predictions of ET, SH, BW, and GPP, while eight features are crucial for predicting AGB and BR_{e2t}. Even though the XGBoost algorithm has an excellent ability to capture complex nonlinear relationships, it does not predict well the PFT competition related variables of AGB and BR_{e2t} because the physical model cannot robustly predict coexisting PFTs due to the higher dimensionality of predicting PFT composition as compared to other ecosystem variables. Another important point worth mentioning is the small sample size of coexistence cases in Exp-CTR, with only 309 cases having BR_{e2t} in the range of [0.1, 0.9], while the majority of cases are dominated by either early or late successional PFT. This limited sample size may not provide enough data to train the XGBoost surrogate model sufficiently for predicting BR_{e2t} within the range of [0.1, 0.9]. Therefore, further studies are still needed to improve the emulation of PFT competition related variables. Other approaches that have been applied in VDMs but not specifically for PFT coexistence modeling, for example, the generalized likelihood uncertainty estimation (GLUE) approach (Zhang et al., 2022) and the Bayesian model emulation approach (Fer et al., 2018), could provide alternative ways. Furthermore, we suggest exploring other machine learning algorithms, such as Gaussian process and neural network algorithms, which may be better suited for capturing non-linear correlations and learning from sparse data.

Overall, our study presents a reproducible approach that utilizes machine learning to identify parameter values that improve model fidelity against observations and promote coexistence between plant functional types in vegetation demography models across diverse ecosystems. This

approach has the potential to enhance the modeling of PFT coexistence in other ecosystems, such as the mixed conifer forests in Sierra Nevada, California (Buotte et al., 2021), Amazon forests subject to selective logging (Huang et al., 2020) and tropical forests with heterogeneous soils and subject to droughts in Panama (Cheng et al., 2021).

4.3 Trait tradeoffs between coexisting PFTs

Trait-related parameters show tradeoffs between early and late successional PFTs for the ELM–FATES simulated coexisting experiments. The relative differences between the two PFTs in SLA, V_{cmax}, and WD complementarily coordinate with the relative difference in M_{bk} and L_{leaf}, hence avoiding competitive exclusion (Figure 9). These ELM-FATES reflected tradeoffs are consistent with the niche-based species coexistence mechanisms of environmental filtering and niche partitioning (MICHALKO and PEKÁR, 2015; Adler et al., 2013). On the one hand, in the coexisting cases, the relative differences between the two PFTs' parameters should not be considerable. For example, a large difference in SLA more likely favors the early cases (green dash box in Figure 9). This is related to environmental filtering in which coexisting species require some degree of convergence in strategy to survive and persist under given environmental conditions (Cadotte and Tucker, 2017; Thakur and Wright, 2017). On the other hand, some degree of differences should exist between the two PFTs' parameters in the coexisting cases. This is related to niche partitioning to ensure either differences in resource requirements or differences in tolerance to surrounding conditions (Kraft et al., 2015; Fowler et al., 2013). Phenomenological evidence has shown that functional trait variation promotes coexistence or increases species richness (Uriarte et al., 2010; Angert et al., 2009; Adler et al., 2006; Mason et al., 2012; Ben-Hur et al., 2012).

In our ELM-FATES simulations, the primary axis of competition for resources is light. The tradeoffs between the two PFTs' parameters differentiate their vertical competition in light absorption, which has been shown to strongly control tropical forest community composition (Farrior et al., 2016; Poorter et al., 2003). Even though the early PFT has a shallower rooting depth than the late PFT, there is no critical dry condition during our simulation period (i.e., corresponding to values of the water stress factor (BTRAN) close to 1.0 in Figure S7). Therefore, competition for water resource access negligibly contributes to PFT coexistence in this study. Previous tropical studies also revealed these coexistence mechanisms. At a tropical forest site in eastern Ecuador, Kraft et al. (2008) found that cooccurring trees are often less ecologically similar, and both environmental filtering (different topographic habitats of ridgetops vs. valley) and niche differentiation simultaneously contribute to species coexistence. Swenson & Enquist (2009) also found that at small spatial scales in a tropical forest, most traits of coexisting species were under-dispersed, consistent with environmental filtering, while the seed mass and maximum height were over-dispersed, reflecting niche partitioning.

4.4 Limitations and further model development

Some limitations exist in our experiments. Niche partitioning is a critical aspect of promoting species coexistence, which is closely related to spatial heterogeneity, temporal heterogeneity, disturbances (e.g., nature enemy, fire), and resource partitioning (Adler et al., 2013). In our current ELM-FATES simulations, some processes that have been or are being developed in the model are not considered. These processes include nutrient limitation (Holm et al., 2020), fire disturbance (Fisher et al., 2015), subsurface lateral flow (Fang et al., 2022), and plant hydraulics (Chitra-Tarak

et al., 2021; Li et al., 2021). Ignoring these processes could limit the potential of niche partitioning among PFT in our ELM-FATES simulations. Topography has been recognized as an essential spatial heterogeneity factor for tropical forests, but it is not considered in ELM-FATES (Kraft et al., 2008; Costa et al., 2022). For example, Fang et al. (2022) coupled a three-dimensional hydrology model (ParFlow) with ELM-FATES and found that lateral flow plays a prominent role in governing aboveground biomass, and Cheng et al. (2021) also found a critical role for subsurface hydrology on coexistence. As these processes are added to the model, the reproducibility aspects of the XGBoost method to identify PFT combinations that match a broad range of criteria will be particularly important.

Lacking other features or processes could also affect PFT coexistence in the current FATES. For example, plant trait plasticity, that plants can adjust their morphological and/or physiological traits to better adapt to the environment (Nicotra et al., 2010; Bloomfield et al., 2018; McDowell et al., 2022), is also not well considered in FATES. Leaf traits such as V_{cmax} and SLA do vary vertically through the canopy in FATES, via a prescribed relationship described by Lloyd et al., 2010. Liu and Ng (2019) found that the SLA of a desert shrub is significantly correlated with seasonal water availability. Additionally, FATES only considers the inter-PFT variance of functional traits (e.g., different V_{cmax} for early and late PFT). However, studies revealed that trait variations commonly exist within and between species (Wright et al., 2005; Engemann et al., 2016; Meng et al., 2015; Dong et al., 2020; Siefert et al., 2015), which play a vital role in maintaining plant diversity (Violle et al., 2012; Lu et al., 2017). Reproductive features that enhance competitive exclusion tendencies have been illustrated to affect coexistence (Maréchaux and Chave, 2017; Fisher et al., 2018). Hanbury-Brown et al. (2022) discussed the importance of the representation of forest regeneration,

including improving parameters and algorithms for reproductive allocation, dispersal, seed survival and germination, environmental filtering in the seedling layer, and tree regeneration strategies adapted to wind, fire, and anthropogenic disturbance regimes. Besides, both growth-survival and stature-recruitment tradeoffs are critical to accurately predict successional patterns in tropical forest structure and competition (see details in Rüger et al., 2020), which should also be better considered in future model development. Furthermore, measured plant traits are increasingly available, e.g., the TRY datasets (Kattge et al., 2020) can be used to improve the model process and parameterizations. Future studies on properly and adequately using these datasets to guide VDM parameterizations are advocated.

4.5 Enhancing VDM prediction with machine learning

We provide a brief overview of how machine learning can be applied to improve the modeling of plant dynamics, specifically in the context of vegetation demographic models. Firstly, ML can be used to derive trait parameter values. For instance, in this study, ML could be applied to replace the simple equations to derive the relationships between measured traits (Section 4.1). By integrating multiple datasets, including in situ measurements, atmospheric forcing, and remote sensing, ML could derive the spatial patterns and temporal variations of trait parameters for use in large-scale VDM modeling. Secondly, ML can be utilized to optimize parameters by developing surrogate models that emulate the relationships between the parameters and the VDM simulations, and using the surrogate models to identify optimal parameter values. This application has demonstrated success in this study and previous studies (e.g., Tsai et al., 2021; Dagon et al., 2020; Watson-Parris et al., 2021). Another benefit of using ML in VDMs is the ability to develop benchmark datasets. For example, studies have successfully employed ML to derive AGB datasets

for various ecosystems (Morais et al., 2021; Zhang et al., 2020; Li et al., 2020; Bispo et al., 2020; Pham et al., 2020). These datasets can serve as benchmarks to evaluate the accuracy of VDM simulations. Lastly, ML can be used to replace semiempirical sub-models with little theoretical bases in DGVMs (Reichstein et al., 2019). For example, accurately modeling wildfire using process-based wildfire models integrated in DGVMs remains challenging. However, ML-based wildfire models have shown advantages in accuracy and computational efficiency (Rodrigues and Riva, 2014; Jain et al., 2020; Sayad et al., 2019), and have the potential to be employed in Earth system models to improve wildfire simulations (e.g., Zhu et al., 2022).

5. Conclusions

In this study, we explored two possible solutions to improve PFT coexistence modeling in a cohort-based model (ELM-FATES): (1) using plant trait relationships established from field measurements and (2) using machine learning surrogate models to optimize trait parameter values. Three ensembles of ELM-FATES experiments were conducted over a tropical forest site at Manaus, Brazil. We found that considering the observed trait relationships (Exp-OBS) slightly improves the simulations of water (ET), energy (SH and BW), and carbon (GPP, AGB) when compared against observations, but degrades the simulation of PFT coexistence. Based on Exp-CTR, the ML surrogate models were built to optimize the ELM-FATES parameters by integrating the observations (i.e., ET, SH, BW, GPP, and AGB) and PFT coexistence criteria. Exp-ML, with parameters selected by the ML surrogate models, vastly improves the simulation of PFT coexistence, and also better reproduces the annual means and seasonal variations of ET, SH, BW, GPP, and the filed inventory of AGB. This study demonstrates the benefits of using machine learning models to improve the modeling of PFT coexistence in ELM-FATES, with important implications for modeling the response and feedback of ecosystem dynamics to climate change. Our results also suggest that the incorporation of additional mechanisms into ELM-FATES is essential for robust modeling of coexisting PFTs.

Code and Data Availability. The ELM-FATES source code, surface and domain data, forcing data, and ML codes used in this study are archived on Zenodo (https://doi.org/10.5281/zenodo.7730685). The observational reference datasets of GPP, ET, SH, BW, and AGB are obtained from Holm et al. (2020). The forcing data are available from Oak Ridge National Laboratory Distributed Active Archive Center (ORNL DAAC), LBA-ECO CD-32 Flux Tower Network Data Compilation, Brazilian Amazon: 1999-2006, V2, https://daac.ornl.gov/LBA/guides/CD32_Fluxes_Brazil.html.

Author contributions. LL and YF designed and conducted the experiments and analysis, and drafted the manuscript. ZZ and MS contributed to the machine learning, experiment design, and improvement of the manuscript. LRL contributed to the interpretation and discussion of results, and improvement of the manuscript. ML, CDK, JAH, RF, NGM, and JC contributed to the dataset, interpretation, discussion, and modification of the manuscript.

Acknowledgments. This research was conducted at Pacific Northwest National Laboratory, operated for the U.S. Department of Energy by Battelle Memorial Institute under contract DE-AC05-76RL01830. This study was supported by the Department of Energy's (DOE) Office of Biological and Environmental Research as part of the Terrestrial Ecosystem Science program through the Next-Generation Ecosystem Experiments (NGEE)-Tropics project. RF acknowledges funding by the European Union's Horizon 2020 (H2020) research and innovation program under Grant Agreement No. 101003536 (ESM2025 – Earth System Models for the Future) and 821003 (4C, Climate-Carbon Interactions in the Coming Century)

Financial support. This research was supported by the U.S. Department of Energy, Office of Science (grant no. 71073).

Competing interests. The authors declare that they have no conflict of interest.

Reference

Adler, P. B., HilleRisLambers, J., Kyriakidis, P. C., Guan, Q., and Levine, J. M.: Climate variability has a stabilizing effect on the coexistence of prairie grasses., P Natl Acad Sci Usa, 103, 12793–8, https://doi.org/10.1073/pnas.0600599103, 2006.

Adler, P. B., Fajardo, A., Kleinhesselink, A. R., and Kraft, N. J. B.: Trait-based tests of coexistence mechanisms, Ecol Lett, 16, 1294–1306, https://doi.org/10.1111/ele.12157, 2013.

Angert, A. L., Huxman, T. E., Chesson, P., and Venable, D. L.: Functional tradeoffs determine species coexistence via the storage effect, Proc National Acad Sci, 106, 11641–11645, https://doi.org/10.1073/pnas.0904512106, 2009.

Antoniadis, A., Lambert-Lacroix, S., and Poggi, J.-M.: Random forests for global sensitivity analysis: A selective review, Reliab Eng Syst Safe, 206, 107312, https://doi.org/10.1016/j.ress.2020.107312, 2020.

Bauman, D., Fortunel, C., Delhaye, G., Malhi, Y., Cernusak, L. A., Bentley, L. P., Rifai, S. W., Aguirre-Gutiérrez, J., Menor, I. O., Phillips, O. L., McNellis, B. E., Bradford, M., Laurance, S. G. W., Hutchinson, M. F., Dempsey, R., Santos-Andrade, P. E., Ninantay-Rivera, H. R., Paucar, J. R. C., and McMahon, S. M.: Tropical tree mortality has increased with rising atmospheric water stress, Nature, 1–6, https://doi.org/10.1038/s41586-022-04737-7, 2022.

Belda, D. M., Anthoni, P., Wårlind, D., Olin, S., Schurgers, G., Tang, J., Smith, B., and Arneth, A.: LPJ-GUESS/LSMv1.0: a next-generation land surface model with high ecological realism, Geosci Model Dev, 15, 6709–6745, https://doi.org/10.5194/gmd-15-6709-2022, 2022.

Ben-Hur, E., Fragman-Sapir, O., Hadas, R., Singer, A., and Kadmon, R.: Functional trade-offs increase species diversity in experimental plant communities, Ecol Lett, 15, 1276–1282, https://doi.org/10.1111/j.1461-0248.2012.01850.x, 2012.

Berzaghi, F., Wright, I. J., Kramer, K., Oddou-Muratorio, S., Bohn, F. J., Reyer, C. P. O., Sabaté, S., Sanders, T. G. M., and Hartig, F.: Towards a New Generation of Trait-Flexible Vegetation Models, Trends Ecol Evol, 35, 191–205, https://doi.org/10.1016/j.tree.2019.11.006, 2019.

Bispo, P. da C., Rodríguez-Veiga, P., Zimbres, B., Miranda, S. do C. de, Cezare, C. H. G., Fleming, S., Baldacchino, F., Louis, V., Rains, D., Garcia, M., Espírito-Santo, F. D. B., Roitman, I., Pacheco-Pascagaza, A. M., Gou, Y., Roberts, J., Barrett, K., Ferreira, L. G., Shimbo, J. Z., Alencar, A., Bustamante, M., Woodhouse, I. H., Sano, E. E., Ometto, J. P., Tansey, K., and Balzter, H.: Woody Aboveground Biomass Mapping of the Brazilian Savanna with a Multi-Sensor and Machine Learning Approach, Remote Sens-basel, 12, 2685, https://doi.org/10.3390/rs12172685, 2020.

Bloomfield, K. J., Cernusak, L. A., Eamus, D., Ellsworth, D. S., Prentice, I. C., Wright, I. J., Boer, M. M., Bradford, M. G., Cale, P., Cleverly, J., Egerton, J. J. G., Evans, B. J., Hayes, L. S., Hutchinson, M. F., Liddell, M. J., Macfarlane, C., Meyer, W. S., Prober, S. M., Togashi, H. F., Wardlaw, T., Zhu, L., and Atkin, O. K.: A continental-scale assessment of variability in leaf traits: Within species, across sites and between seasons, Funct Ecol, 32, 1492–1506, https://doi.org/10.1111/1365-2435.13097, 2018.

Bonan, G. B.: Forests and Climate Change: Forcings, Feedbacks, and the Climate Benefits of Forests, Science, 320, 1444–1449, https://doi.org/10.1126/science.1155121, 2008.

Breiman, L.: Random Forests, Mach Learn, 45, 5–32, https://doi.org/10.1023/a:1010933404324, 2001.

Brister, E., Newhouse, A. E., and Texas, C. for E. P., The University of North: Not the Same Old Chestnut: Rewilding Forests with Biotechnology, Environ Ethics, 42, 149–167, https://doi.org/10.5840/enviroethics2020111614, 2020.

Buotte, P. C., Koven, C. D., Xu, C., Shuman, J. K., Goulden, M. L., Levis, S., Katz, J., Ding, J., Ma, W., Robbins, Z., and Kueppers, L. M.: Capturing functional strategies and compositional dynamics in vegetation demographic models, Biogeosciences, 18, 4473–4490, https://doi.org/10.5194/bg-18-4473-2021, 2021.

Cadotte, M. W. and Tucker, C. M.: Should Environmental Filtering be Abandoned?, Trends Ecol Evol, 32, 429–437, https://doi.org/10.1016/j.tree.2017.03.004, 2017.

Cao, M. and Woodward, F. I.: Dynamic responses of terrestrial ecosystem carbon cycling to global climate change, Nature, 393, 249–252, https://doi.org/10.1038/30460, 1998.

Chen, T. and Guestrin, C.: XGBoost: A Scalable Tree Boosting System, Proc 22nd Acm Sigkdd Int Conf Knowl Discov Data Min, 785–794, https://doi.org/10.1145/2939672.2939785, 2016.

Cheng, Y., Leung, L. R., Huang, M., Koven, C., Detto, M., Knox, R., Bisht, G., Bretfeld, M., and Fisher, R. A.: Modeling the joint effects of vegetation characteristics and soil properties on ecosystem dynamics in a Panama tropical forest, J Adv Model Earth Sy, https://doi.org/10.1029/2021ms002603, 2021.

Chitra-Tarak, R., Xu, C., Aguilar, S., Anderson-Teixeira, K. J., Chambers, J., Detto, M., Faybishenko, B., Fisher, R. A., Knox, R. G., Koven, C. D., Kueppers, L. M., Kunert, N., Kupers, S. J., McDowell, N. G., Newman, B. D., Paton, S. R., Pérez, R., Ruiz, L., Sack, L., Warren, J. M., Wolfe, B. T., Wright, C., Wright, S. J., Zailaa, J., and McMahon, S. M.: Hydraulically-vulnerable trees survive on deep-water access during droughts in a tropical forest, New Phytol, 231, 1798–1813, https://doi.org/10.1111/nph.17464, 2021.

Christoffersen, B. O., Gloor, M., Fauset, S., Fyllas, N. M., Galbraith, D. R., Baker, T. R., Kruijt, B., Rowland, L., Fisher, R. A., Binks, O. J., Sevanto, S., Xu, C., Jansen, S., Choat, B., Mencuccini, M., McDowell, N. G., and Meir, P.: Linking hydraulic traits to tropical forest

function in a size-structured and trait-driven model (TFS v.1-Hydro), Geoscientific Model Development, 9, 4227–4255, https://doi.org/10.5194/gmd-9-4227-2016, 2016.

Costa, F. R. C., Schietti, J., Stark, S. C., and Smith, M. N.: The other side of tropical forest drought: do shallow water table regions of Amazonia act as large-scale hydrological refugia from drought?, New Phytol, https://doi.org/10.1111/nph.17914, 2022.

Dagon, K., Sanderson, B. M., Fisher, R. A., and Lawrence, D. M.: A machine learning approach to emulation and biophysical parameter estimation with the Community Land Model, version 5, Adv Statistical Clim Meteorology Oceanogr, 6, 223–244, https://doi.org/10.5194/ascmo-6-223-2020, 2020.

Díaz, S., Kattge, J., Cornelissen, J. H. C., Wright, I. J., Lavorel, S., Dray, S., Reu, B., Kleyer, M., Wirth, C., Prentice, I. C., Garnier, E., Bönisch, G., Westoby, M., Poorter, H., Reich, P. B., Moles, A. T., Dickie, J., Gillison, A. N., Zanne, A. E., Chave, J., Wright, S. J., Sheremet'ev, S. N., Jactel, H., Baraloto, C., Cerabolini, B., Pierce, S., Shipley, B., Kirkup, D., Casanoves, F., Joswig, J. S., Günther, A., Falczuk, V., Rüger, N., Mahecha, M. D., and Gorné, L. D.: The global spectrum of plant form and function, Nature, 529, 167–171, https://doi.org/10.1038/nature16489, 2016.

Domingues, T. F., Berry, J. A., Martinelli, L. A., Ometto, J. P. H. B., and Ehleringer, J. R.: Parameterization of Canopy Structure and Leaf-Level Gas Exchange for an Eastern Amazonian Tropical Rain Forest (Tapajós National Forest, Pará, Brazil), Earth Interact, 9, 1–23, https://doi.org/10.1175/ei149.1, 2005.

Dong, N., Prentice, I. C., Wright, I. J., Evans, B. J., Togashi, H. F., Caddy-Retalic, S., McInerney, F. A., Sparrow, B., Leitch, E., and Lowe, A. J.: Components of leaf-trait variation along environmental gradients, New Phytol, 228, 82–94, https://doi.org/10.1111/nph.16558, 2020.

Duan, Q., Sorooshian, S., and Gupta, V.: Effective and efficient global optimization for conceptual rainfall-runoff models, Water Resour Res, 28, 1015–1031, https://doi.org/10.1029/91wr02985, 1992.

Engemann, K., Sandel, B., Boyle, B., Enquist, B. J., Jørgensen, P. M., Kattge, J., McGill, B. J., Morueta-Holme, N., Peet, R. K., Spencer, N. J., Violle, C., Wiser, S. K., and Svenning, J.-C.: A plant growth form dataset for the New World., Ecology, 97, 3243–3243, https://doi.org/10.1002/ecy.1569, 2016.

Fang, Y., Leung, L. R., Duan, Z., Wigmosta, M. S., Maxwell, R. M., Chambers, J. Q., and Tomasella, J.: Influence of landscape heterogeneity on water available to tropical forests in an Amazonian catchment and implications for modeling drought response, Journal of Geophysical Research: Atmospheres, 122, 8410–8426, https://doi.org/10.1002/2017jd027066, 2017.

Fang, Y., Leung, R., Koven, C., Bisht, G., Detto, M., Cheng, Y., McDowell, N., Muller-Landau, H., Wright, S. J., and Chambers, J.: Modeling the topographic influence on aboveground

915 biomass using a coupled model of hillslope hydrology and ecosystem dynamics, Geoscientific
916 Model Dev Discuss, 2022, 1–41, https://doi.org/10.5194/gmd-2022-148, 2022.

917 Farrior, C. E., Bohlman, S. A., Hubbell, S., and Pacala, S. W.: Dominance of the suppressed:
918 Power-law size structure in tropical forests, Science, 351, 155–157,
919 https://doi.org/10.1126/science.aad0592, 2016.

920 Feeley, K. J., Davies, S. J., Ashton, P. S., Bunyavejchewin, S., Supardi, M. N. N., Kassim, A. R.,
921 Tan, S., and Chave, J.: The role of gap phase processes in the biomass dynamics of tropical
922 forests, Proc Royal Soc B Biological Sci, 274, 2857–2864,
923 https://doi.org/10.1098/rspb.2007.0954, 2007.

924 Feigl, M., Lebiedzinski, K., Herrnegger, M., and Schulz, K.: Machine-learning methods for
925 stream water temperature prediction, Hydrol Earth Syst Sc, 25, 2951–2977,
926 https://doi.org/10.5194/hess-25-2951-2021, 2021.

927 Fer, I., Kelly, R., Moorcroft, P. R., Richardson, A. D., Cowdery, E. M., and Dietze, M. C.:
928 Linking big models to big data: efficient ecosystem model calibration through Bayesian model
929 emulation, Biogeosciences, 15, 5801–5830, https://doi.org/10.5194/bg-15-5801-2018, 2018.

930 Fisher, R., McDowell, N., Purves, D., Moorcroft, P., Sitch, S., Cox, P., Huntingford, C., Meir, P.,
931 and Woodward, F. I.: Assessing uncertainties in a second-generation dynamic vegetation model
932 caused by ecological scale limitations, New Phytol, 187, 666–681,
933 https://doi.org/10.1111/j.1469-8137.2010.03340.x, 2010.

934 Fisher, R. A., Muszala, S., Verteinstein, M., Lawrence, P., Xu, C., McDowell, N. G., Knox, R.
935 G., Koven, C., Holm, J., Rogers, B. M., Spessa, A., Lawrence, D., and Bonan, G.: Taking off the
936 training wheels: the properties of a dynamic vegetation model without climate envelopes,
937 CLM4.5(ED), Geosci Model Dev, 8, 3593–3619, https://doi.org/10.5194/gmd-8-3593-2015,
938 2015.

939 Fisher, R. A., Koven, C. D., Anderegg, W. R. L., Christoffersen, B. O., Dietze, M. C., Farrior, C.
940 E., Holm, J. A., Hurtt, G. C., Knox, R. G., Lawrence, P. J., Lichstein, J. W., Longo, M.,
941 Matheny, A. M., Medvigy, D., Muller-Landau, H. C., Powell, T. L., Serbin, S. P., Sato, H.,
942 Shuman, J. K., Smith, B., Trugman, A. T., Viskari, T., Verbeeck, H., Weng, E., Xu, C., Xu, X.,
943 Zhang, T., and Moorcroft, P. R.: Vegetation demographics in Earth System Models: A review of
944 progress and priorities, Global Change Biol, 24, 35–54, https://doi.org/10.1111/gcb.13910, 2018.

945 Foken, T.: THE ENERGY BALANCE CLOSURE PROBLEM: AN OVERVIEW, Ecol Appl,
946 18, 1351–1367, https://doi.org/10.1890/06-0922.1, 2008.

947 Foley, J. A., Prentice, I. C., Ramankutty, N., Levis, S., Pollard, D., Sitch, S., and Haxeltine, A.:
948 An integrated biosphere model of land surface processes, terrestrial carbon balance, and
949 vegetation dynamics, Global Biogeochem Cy, 10, 603–628, https://doi.org/10.1029/96gb02692,
950 1996.

951 Fowler, D., Lessard, J.-P., and Sanders, N. J.: Niche filtering rather than partitioning shapes the
952 structure of temperate forest ant communities., J Animal Ecol, 83, 943–52,
953 https://doi.org/10.1111/1365-2656.12188, 2013.

954 Friedman, J. H.: Greedy function approximation: A gradient boosting machine., Ann Statistics,
955 29, https://doi.org/10.1214/aos/1013203451, 2001.

956 Fyllas, N. M., Gloor, E., Mercado, L. M., Sitch, S., Quesada, C. A., Domingues, T. F., Galbraith,
957 D. R., Torre-Lezama, A., Vilanova, E., Ramírez-Angulo, H., Higuchi, N., Neill, D. A., Silveira,
958 M., Ferreira, L., C, G. A. A., MALHI, Y., Phillips, O. L., and Lloyd, J.: Analysing Amazonian
959 forest productivity using a new individual and trait-based model (TFS v.1), Geoscientific Model
960 Development, 7, 1251–1269, https://doi.org/10.5194/gmd-7-1251-2014, 2014.

961 Gatti, L. V., Basso, L. S., Miller, J. B., Gloor, M., Domingues, L. G., Cassol, H. L. G., Tejada,
962 G., Aragão, L. E. O. C., Nobre, C., Peters, W., Marani, L., Arai, E., Sanches, A. H., Corrêa, S.
963 M., Anderson, L., Randow, C. V., Correia, C. S. C., Crispim, S. P., and Neves, R. A. L.:
964 Amazonia as a carbon source linked to deforestation and climate change, Nature, 595, 388–393,
965 https://doi.org/10.1038/s41586-021-03629-6, 2021.

966 Golaz, J., Caldwell, P. M., Roekel, L. P. V., Petersen, M. R., Tang, Q., Wolfe, J. D., Abeshu, G.,
967 Anantharaj, V., Asay-Davis, X. S., Bader, D. C., Baldwin, S. A., Bisht, G., Bogenschutz, P. A.,
968 Branstetter, M., Brunke, M. A., Brus, S. R., Burrows, S. M., Cameron-Smith, P. J., Donahue, A.
969 S., Deakin, M., Easter, R. C., Evans, K. J., Feng, Y., Flanner, M., Foucar, J. G., Fyke, J. G.,
970 Griffin, B. M., Hannay, C., Harrop, B. E., Hoffman, M. J., Hunke, E. C., Jacob, R. L., Jacobsen,
971 D. W., Jeffery, N., Jones, P. W., Keen, N. D., Klein, S. A., Larson, V. E., Leung, L. R., Li, H.,
972 Lin, W., Lipscomb, W. H., Ma, P., Mahajan, S., Maltrud, M. E., Mametjanov, A., McClean, J.
973 L., McCoy, R. B., Neale, R. B., Price, S. F., Qian, Y., Rasch, P. J., Eyre, J. E. J. R., Riley, W. J.,
974 Ringler, T. D., Roberts, A. F., Roesler, E. L., Salinger, A. G., Shaheen, Z., Shi, X., Singh, B.,
975 Tang, J., Taylor, M. A., Thornton, P. E., Turner, A. K., Veneziani, M., Wan, H., Wang, H.,
976 Wang, S., Williams, D. N., Wolfram, P. J., Worley, P. H., Xie, S., Yang, Y., Yoon, J., Zelinka,
977 M. D., Zender, C. S., Zeng, X., Zhang, C., Zhang, K., Zhang, Y., Zheng, X., Zhou, T., and Zhu,
978 Q.: The DOE E3SM Coupled Model Version 1: Overview and Evaluation at Standard
979 Resolution, J Adv Model Earth Sy, 11, 2089–2129, https://doi.org/10.1029/2018ms001603,
980 2019.

981 Hanbury-Brown, A. R., Ward, R. E., and Kueppers, L. M.: Forest regeneration within Earth
982 system models: current process representations and ways forward, New Phytol, 235, 20–40,
983 https://doi.org/10.1111/nph.18131, 2022.

984 Haverd, V., Smith, B., Cook, G. D., Briggs, P. R., Nieradzik, L., Roxburgh, S. H., Liedloff, A.,
985 Meyer, C. P., and Canadell, J. G.: A stand-alone tree demography and landscape structure
986 module for Earth system models, Geophys Res Lett, 40, 5234–5239,
987 https://doi.org/10.1002/grl.50972, 2013.

He, X., Liu, S., Xu, T., Yu, K., Gentine, P., Zhang, Z., Xu, Z., Jiao, D., and Wu, D.: Improving predictions of evapotranspiration by integrating multi-source observations and land surface model, Agr Water Manage, 272, 107827, https://doi.org/10.1016/j.agwat.2022.107827, 2022.

Holm, J. A., Knox, R. G., Zhu, Q., Fisher, R. A., Koven, C. D., Lima, A. J. N., Riley, W. J., Longo, M., Negrón-Juárez, R. I., Araujo, A. C., Kueppers, L. M., Moorcroft, P. R., Higuchi, N., and Chambers, J. Q.: The Central Amazon Biomass Sink Under Current and Future Atmospheric CO2: Predictions From Big-Leaf and Demographic Vegetation Models, J Geophys Res Biogeosciences, 125, https://doi.org/10.1029/2019jg005500, 2020.

Huang, M., Xu, Y., Longo, M., Keller, M., Knox, R. G., Koven, C. D., and Fisher, R. A.: Assessing impacts of selective logging on water, energy, and carbon budgets and ecosystem dynamics in Amazon forests using the Functionally Assembled Terrestrial Ecosystem Simulator, Biogeosciences, 17, 4999–5023, https://doi.org/10.5194/bg-17-4999-2020, 2020.

Hubau, W., Lewis, S. L., Phillips, O. L., Affum-Baffoe, K., Beeckman, H., Cuní-Sanchez, A., Daniels, A. K., Ewango, C. E. N., Fauset, S., Mukinzi, J. M., SHEIL, D., Sonké, B., Sullivan, M. J. P., Sunderland, T. C. H., Taedoumg, H., Thomas, S. C., White, L. J. T., Abernethy, K. A., Adu-Bredu, S., Amani, C. A., Baker, T. R., Banin, L. F., Baya, F., Begne, S. K., Bennett, A. C., Benedet, F., Bitariho, R., Bocko, Y. E., Boeckx, P., Boundja, P., Brienen, R. J. W., Brncic, T., Chezeaux, E., Chuyong, G. B., Clark, C. J., Collins, M., Comiskey, J. A., Coomes, D. A., Dargie, G. C., Haulleville, T. de, Kamdem, M. N. D., Doucet, J.-L., Esquivel-Muelbert, A., Feldpausch, T. R., Fofanah, A., Foli, E. G., Gilpin, M., Gloor, E., Gonmadje, C., Gourlet-Fleury, S., Hall, J. S., Hamilton, A. C., Harris, D. J., Hart, T. B., Hockemba, M. B. N., Hladik, A., Ifo, S. A., Jeffery, K. J., Jucker, T., Yakusu, E. K., Kearsley, E., Kenfack, D., Koch, A., Leal, M. E., Levesley, A., Lindsell, J. A., Lisingo, J., González, G. L., Lovett, J. C., Makana, J.-R., Malhi, Y., Marshall, A. R., Martin, J., Martin, E. H., Mbayu, F. M., Medjibe, V. P., Mihindou, V., Mitchard, E. T. A., Moore, S., Munishi, P. K. T., Bengone, N. N., Ojo, L., Ondo, F. E., Peh, K. S. H., Pickavance, G. C., Poulsen, A. D., Poulsen, J. R., Qie, L., Reitsma, J., Rovero, F., Swaine, M. D., Talbot, J., Taplin, J., Taylor, D. M., Thomas, D. W., Toirambe, B., Mukendi, J. T., Tuagben, D., Umunay, P. M., et al.: Asynchronous carbon sink saturation in African and Amazonian tropical forests, Nature, 579, 80–87, https://doi.org/10.1038/s41586-020-2035-0, 2020.

Hurtt, G. C., Moorcroft, PauL. R., And, S. W. P., and Levin, S. A.: Terrestrial models and global change: challenges for the future, Global Change Biol, 4, 581–590, https://doi.org/10.1046/j.1365-2486.1998.t01-1-00203.x, 1998.

Jain, P., Coogan, S. C. P., Subramanian, S. G., Crowley, M., Taylor, S., and Flannigan, M. D.: A review of machine learning applications in wildfire science and management, Arxiv, https://doi.org/10.48550/arxiv.2003.00646, 2020.

Jonard, M., André, F., Coligny, F. de, Wergifosse, L. de, Beudez, N., Davi, H., Ligot, G., Ponette, Q., and Vincke, C.: HETEROFOR 1.0: a spatially explicit model for exploring the response of structurally complex forests to uncertain future conditions – Part 1: Carbon fluxes

and tree dimensional growth, Geosci Model Dev, 13, 905–935, https://doi.org/10.5194/gmd-13-905-2020, 2020.

Jung, M., Koirala, S., Weber, U., Ichii, K., Gans, F., Camps-Valls, G., Papale, D., Schwalm, C., Tramontana, G., and Reichstein, M.: The FLUXCOM ensemble of global land-atmosphere energy fluxes., Sci Data, 6, 74, https://doi.org/10.1038/s41597-019-0076-8, 2019.

Kattge, J., Bönisch, G., Díaz, S., Lavorel, S., Prentice, I. C., Leadley, P., Tautenhahn, S., Werner, G. D. A., Aakala, T., Abedi, M., Acosta, A. T. R., Adamidis, G. C., Adamson, K., Aiba, M., Albert, C. H., Alcántara, J. M., C, C. A., Aleixo, I., Ali, H., Amiaud, B., Ammer, C., Amoroso, M. M., Anand, M., Anderson, C., Anten, N., Antos, J., Apgaua, D. M. G., Ashman, T. L., Asmara, D. H., Asner, G. P., Aspinwall, M., Atkin, O., Aubin, I., Spohr, L. B., Bahalkeh, K., Bahn, M., Baker, T., Baker, W. J., Bakker, J. P., Baldocchi, D., Baltzer, J., Banerjee, A., Baranger, A., Barlow, J., Barneche, D. R., Baruch, Z., Bastianelli, D., Battles, J., Bauerle, W., Bauters, M., Bazzato, E., Beckmann, M., Beeckman, H., Beierkuhnlein, C., Bekker, R., Belfry, G., Belluau, M., Beloiu, M., Benavides, R., Benomar, L., Lattke, M. L. B., Berenguer, E., Bergamin, R., Bergmann, J., Carlucci, M. B., Berner, L., Römermann, M. B., Bigler, C., Bjorkman, A. D., Blackman, C., Blanco, C., Blonder, B., Blumenthal, D., González, K. T. B., Boeckx, P., Bohlman, S., Gaese, K. B., Marsh, L. B., Bond, W., Bond-Lamberty, B., Boom, A., Boonman, C. C. F., Bordin, K., Boughton, E. H., Boukili, V., Bowman, D. M. J. S., Bravo, S., Brendel, M. R., Broadley, M. R., Brown, K. A., Bruelheide, H., Brumnich, F., Bruun, H. H., Bruy, D., Buchanan, S. W., Bucher, S. F., Buchmann, N., Buitenwerf, R., Bunker, D. E., et al.: TRY plant trait database – enhanced coverage and open access, Global Change Biology, 26, 119–188, https://doi.org/10.1111/gcb.14904, 2020.

Koven, C. D., Knox, R. G., Fisher, R. A., Chambers, J. Q., Christoffersen, B. O., Davies, S. J., Detto, M., Dietze, M. C., Faybishenko, B., Holm, J., Huang, M., Kovenock, M., Kueppers, L. M., Lemieux, G., Massoud, E., McDowell, N. G., Muller-Landau, H. C., Needham, J. F., Norby, R. J., Powell, T., Rogers, A., Serbin, S. P., Shuman, J. K., Swann, A. L. S., Varadharajan, C., Walker, A. P., Wright, S. J., and Xu, C.: Benchmarking and parameter sensitivity of physiological and vegetation dynamics using the Functionally Assembled Terrestrial Ecosystem Simulator (FATES) at Barro Colorado Island, Panama, Biogeosciences, 17, 3017–3044, https://doi.org/10.5194/bg-17-3017-2020, 2020.

Kraft, N. J. B., Valencia, R., and Ackerly, D. D.: Functional Traits and Niche-Based Tree Community Assembly in an Amazonian Forest, Science, 322, 580–582, https://doi.org/10.1126/science.1160662, 2008.

Kraft, N. J. B., Adler, P. B., Godoy, O., James, E. C., Fuller, S., and Levine, J. M.: Community assembly, coexistence and the environmental filtering metaphor, Funct Ecol, 29, 592–599, https://doi.org/10.1111/1365-2435.12345, 2015.

Lambert, M. S. A., Tang, H., Aas, K. S., Stordal, F., Fisher, R. A., Fang, Y., Ding, J., and Parmentier, F.-J. W.: Inclusion of a cold hardening scheme to represent frost tolerance is essential to model realistic plant hydraulics in the Arctic–boreal zone in CLM5.0-FATES-Hydro, Geosci Model Dev, 15, 8809–8829, https://doi.org/10.5194/gmd-15-8809-2022, 2022.

1067 Lawrence, D. M., Fisher, R. A., Koven, C. D., Oleson, K. W., Swenson, S. C., Bonan, G.,
1068 Collier, N., Ghimire, B., Kampenhout, L., Kennedy, D., Kluzek, E., Lawrence, P. J., Li, F., Li,
1069 H., Lombardozzi, D., Riley, W. J., Sacks, W. J., Shi, M., Vertenstein, M., Wieder, W. R., Xu, C.,
1070 Ali, A. A., Badger, A. M., Bisht, G., Broeke, M., Brunke, M. A., Burns, S. P., Buzan, J., Clark,
1071 M., Craig, A., Dahlin, K., Drewniak, B., Fisher, J. B., Flanner, M., Fox, A. M., Gentine, P.,
1072 Hoffman, F., Keppel-Aleks, G., Knox, R., Kumar, S., Lenaerts, J., Leung, L. R., Lipscomb, W.
1073 H., Lu, Y., Pandey, A., Pelletier, J. D., Perket, J., Randerson, J. T., Ricciuto, D. M., Sanderson,
1074 B. M., Slater, A., Subin, Z. M., Tang, J., Thomas, R. Q., Martin, M. V., and Zeng, X.: The
1075 Community Land Model Version 5: Description of New Features, Benchmarking, and Impact of
1076 Forcing Uncertainty, J Adv Model Earth Sy, 11, 4245–4287,
1077 https://doi.org/10.1029/2018ms001583, 2019.

1078 Leung, L. R., Bader, D. C., Taylor, M. A., and McCoy, R. B.: An Introduction to the E3SM
1079 Special Collection: Goals, Science Drivers, Development, and Analysis, J Adv Model Earth Sy,
1080 12, https://doi.org/10.1029/2019ms001821, 2020.

1081 Li, L., Yang, Z., Matheny, A. M., Zheng, H., Swenson, S. C., Lawrence, D. M., Barlage, M.,
1082 Yan, B., McDowell, N. G., and Leung, L. R.: Representation of Plant Hydraulics in the Noah-
1083 MP Land Surface Model: Model Development and Multiscale Evaluation, J Adv Model Earth
1084 Sy, 13, https://doi.org/10.1029/2020ms002214, 2021.

1085 Li, Y., Li, M., Li, C., and Liu, Z.: Forest aboveground biomass estimation using Landsat 8 and
1086 Sentinel-1A data with machine learning algorithms, Sci Rep-uk, 10, 9952,
1087 https://doi.org/10.1038/s41598-020-67024-3, 2020.

1088 Liu, S. and Ng, G.-H. C.: A data-conditioned stochastic parameterization of temporal plant trait
1089 variability in an ecohydrological model and the potential for plasticity, Agr Forest Meteorol, 274,
1090 184–194, https://doi.org/10.1016/j.agrformet.2019.05.005, 2019.

1091 Longo, M., Knox, R. G., Medvigy, D. M., Levine, N. M., Dietze, M. C., Kim, Y., Swann, A. L.
1092 S., Zhang, K., Rollinson, C. R., Bras, R. L., Wofsy, S. C., and Moorcroft, P. R.: The biophysics,
1093 ecology, and biogeochemistry of functionally diverse, vertically and horizontally heterogeneous
1094 ecosystems: the Ecosystem Demography model, version 2.2 – Part 1: Model description, Geosci
1095 Model Dev, 12, 4309–4346, https://doi.org/10.5194/gmd-12-4309-2019, 2019.

1096 Longo, M., Saatchi, S., Keller, M., Bowman, K., Ferraz, A., Moorcroft, P. R., Morton, D. C.,
1097 Bonal, D., Brando, P., Burban, B., Derroire, G., dos-Santos, M. N., Meyer, V., Saleska, S.,
1098 Trumbore, S., and Vincent, G.: Impacts of Degradation on Water, Energy, and Carbon Cycling
1099 of the Amazon Tropical Forests, J Geophys Res Biogeosciences, 125, e2020JG005677,
1100 https://doi.org/10.1029/2020jg005677, 2020.

1101 Lu, X., Wang, Y., Wright, I. J., Reich, P. B., Shi, Z., and Dai, Y.: Incorporation of plant traits in
1102 a land surface model helps explain the global biogeographical distribution of major forest
1103 functional types, Global Ecol Biogeogr, 26, 304–317, https://doi.org/10.1111/geb.12535, 2017.

1104 Lundberg, S. and Lee, S.-I.: A Unified Approach to Interpreting Model Predictions, Arxiv, 2017.

Lundberg, S. M., Nair, B., Vavilala, M. S., Horibe, M., Eisses, M. J., Adams, T., Liston, D. E., Low, D. K.-W., Newman, S.-F., Kim, J., and Lee, S.-I.: Explainable machine-learning predictions for the prevention of hypoxaemia during surgery, Nat Biomed Eng, 2, 749–760, https://doi.org/10.1038/s41551-018-0304-0, 2018.

Lundberg, S. M., Erion, G., Chen, H., DeGrave, A., Prutkin, J. M., Nair, B., Katz, R., Himmelfarb, J., Bansal, N., and Lee, S.-I.: From local explanations to global understanding with explainable AI for trees, Nat Mach Intell, 2, 56–67, https://doi.org/10.1038/s42256-019-0138-9, 2020.

Ma, L., Hurtt, G., Ott, L., Sahajpal, R., Fisk, J., Lamb, R., Tang, H., Flanagan, S., Chini, L., Chatterjee, A., and Sullivan, J.: Global Evaluation of the Ecosystem Demography Model (ED v3.0), Geoscientific Model Dev Discuss, 2021, 1–41, https://doi.org/10.5194/gmd-2021-292, 2021.

Maréchaux, I. and Chave, J.: An individual-based forest model to jointly simulate carbon and tree diversity in Amazonia: description and applications, Ecol Monogr, 87, 632–664, https://doi.org/10.1002/ecm.1271, 2017.

Mason, N. W. H., Richardson, S. J., Peltzer, D. A., Bello, F. de, Wardle, D. A., and Allen, R. B.: Changes in coexistence mechanisms along a long-term soil chronosequence revealed by functional trait diversity: Functional diversity along ecological gradients, J Ecol, 100, 678–689, https://doi.org/10.1111/j.1365-2745.2012.01965.x, 2012.

Mckay, M. D., Beckman, R. J., and Conover, W. J.: A Comparison of Three Methods for Selecting Values of Input Variables in the Analysis of Output From a Computer Code, Technometrics, 42, 55–61, https://doi.org/10.1080/00401706.2000.10485979, 2000.

McDowell, N. G., Allen, C. D., Anderson-Teixeira, K., Aukema, B. H., Bond-Lamberty, B., Chini, L., Clark, J. S., Dietze, M., Grossiord, C., Hanbury-Brown, A., Hurtt, G. C., Jackson, R. B., Johnson, D. J., Kueppers, L., Lichstein, J. W., Ogle, K., Poulter, B., Pugh, T. A. M., Seidl, R., Turner, M. G., Uriarte, M., Walker, A. P., and Xu, C.: Pervasive shifts in forest dynamics in a changing world, Science, 368, https://doi.org/10.1126/science.aaz9463, 2020.

McDowell, N. G., Sapes, G., Pivovaroff, A., Adams, H. D., Allen, C. D., Anderegg, W. R. L., Arend, M., Breshears, D. D., Brodribb, T., Choat, B., Cochard, H., Cáceres, M. D., Kauwe, M. G. D., Grossiord, C., Hammond, W. M., Hartmann, H., Hoch, G., Kahmen, A., Klein, T., Mackay, D. S., Mantova, M., Martínez-Vilalta, J., Medlyn, B. E., Mencuccini, M., Nardini, A., Oliveira, R. S., Sala, A., Tissue, D. T., Torres-Ruiz, J. M., Trowbridge, A. M., Trugman, A. T., Wiley, E., and Xu, C.: Mechanisms of woody-plant mortality under rising drought, CO2 and vapour pressure deficit, Nat Rev Earth Environ, 3, 294–308, https://doi.org/10.1038/s43017-022-00272-1, 2022.

McMahon, S. M., Harrison, S. P., Armbruster, W. S., Bartlein, P. J., Beale, C. M., Edwards, M. E., Kattge, J., Midgley, G., Morin, X., and Prentice, I. C.: Improving assessment and modelling

of climate change impacts on global terrestrial biodiversity, Trends Ecol Evol, 26, 249–259, https://doi.org/10.1016/j.tree.2011.02.012, 2011.

Medvigy, D., Wofsy, S. C., Munger, J. W., Hollinger, D. Y., and Moorcroft, P. R.: Mechanistic scaling of ecosystem function and dynamics in space and time: Ecosystem Demography model version 2, J Geophys Res Biogeosciences 2005 2012, 114, https://doi.org/10.1029/2008jg000812, 2009.

Meng, T.-T., Wang, H., Harrison, S. P., Prentice, I. C., Ni, J., and Wang, G.: Responses of leaf traits to climatic gradients: adaptive variation versus compositional shifts, Biogeosciences, 12, 5339–5352, https://doi.org/10.5194/bg-12-5339-2015, 2015.

MICHALKO, R. and PEKÁR, S.: Niche partitioning and niche filtering jointly mediate the coexistence of three closely related spider species (Araneae, Philodromidae), Ecol Entomol, 40, 22–33, https://doi.org/10.1111/een.12149, 2015.

Mitchard, E. T. A.: The tropical forest carbon cycle and climate change, Nature, 559, 527–534, https://doi.org/10.1038/s41586-018-0300-2, 2018.

Moorcroft, P. R.: Recent advances in ecosystem-atmosphere interactions: an ecological perspective, Proc Royal Soc Lond Ser B Biological Sci, 270, 1215–1227, https://doi.org/10.1098/rspb.2002.2251, 2003.

Moorcroft, P. R., Hurtt, G. C., and Pacala, S. W.: A Method for Scaling Vegetation Dynamics: The Ecosystem Demography Model (ED), Ecol Monogr, 71, 557, https://doi.org/10.2307/3100036, 2001.

Mora, C., Tittensor, D. P., Adl, S., Simpson, A. G. B., and Worm, B.: How Many Species Are There on Earth and in the Ocean?, Plos Biol, 9, e1001127, https://doi.org/10.1371/journal.pbio.1001127, 2011.

Morais, T. G., Teixeira, R. F. M., Figueiredo, M., and Domingos, T.: The use of machine learning methods to estimate aboveground biomass of grasslands: A review, Ecol Indic, 130, 108081, https://doi.org/10.1016/j.ecolind.2021.108081, 2021.

Nearing, G. S., Kratzert, F., Sampson, A. K., Pelissier, C. S., Klotz, D., Frame, J. M., Prieto, C., and Gupta, H. V.: What Role Does Hydrological Science Play in the Age of Machine Learning?, Water Resour Res, 57, https://doi.org/10.1029/2020wr028091, 2021.

Nicotra, A. B., Atkin, O. K., Bonser, S. P., Davidson, A. M., Finnegan, E. J., Mathesius, U., Poot, P., Purugganan, M. D., Richards, C. L., Valladares, F., and Kleunen, M. van: Plant phenotypic plasticity in a changing climate, Trends Plant Sci, 15, 684–692, https://doi.org/10.1016/j.tplants.2010.09.008, 2010.

Oliveira, R. S., Eller, C. B., Barros, F. de V., Hirota, M., Brum, M., and Bittencourt, P.: Linking plant hydraulics and the fast–slow continuum to understand resilience to drought in tropical ecosystems, New Phytol, 230, 904–923, https://doi.org/10.1111/nph.17266, 2021.

Padarian, J., McBratney, A. B., and Minasny, B.: Game theory interpretation of digital soil mapping convolutional neural networks, Soil, 6, 389–397, https://doi.org/10.5194/soil-6-389-2020, 2020.

Pal, A., Mahajan, S., and Norman, M. R.: Using Deep Neural Networks as Cost-Effective Surrogate Models for Super-Parameterized E3SM Radiative Transfer, Geophys Res Lett, 46, 6069–6079, https://doi.org/10.1029/2018gl081646, 2019.

Peatier, S., Sanderson, B. M., Terray, L., and Roehrig, R.: Investigating Parametric Dependence of Climate Feedbacks in the Atmospheric Component of CNRM-CM6-1, Geophys Res Lett, 49, https://doi.org/10.1029/2021gl095084, 2022.

Pham, T. D., Yokoya, N., Xia, J., Ha, N. T., Le, N. N., Nguyen, T. T. T., Dao, T. H., Vu, T. T. P., Pham, T. D., and Takeuchi, W.: Comparison of Machine Learning Methods for Estimating Mangrove Above-Ground Biomass Using Multiple Source Remote Sensing Data in the Red River Delta Biosphere Reserve, Vietnam, Remote Sens-basel, 12, 1334, https://doi.org/10.3390/rs12081334, 2020.

Piao, S., Wang, X., Wang, K., Li, X., Bastos, A., Canadell, J. G., Ciais, P., Friedlingstein, P., and Sitch, S.: Interannual variation of terrestrial carbon cycle: Issues and perspectives, Global Change Biology, 26, 300–318, https://doi.org/10.1111/gcb.14884, 2020.

Poorter, L., Bongers, F., Sterck, F. J., and Wöll, H.: ARCHITECTURE OF 53 RAIN FOREST TREE SPECIES DIFFERING IN ADULT STATURE AND SHADE TOLERANCE, Ecology, 84, 602–608, https://doi.org/10.1890/0012-9658(2003)084[0602:aorfts]2.0.co;2, 2003.

Purves, D. W., Lichstein, J. W., Strigul, N., and Pacala, S. W.: Predicting and understanding forest dynamics using a simple tractable model, Proc National Acad Sci, 105, 17018–17022, https://doi.org/10.1073/pnas.0807754105, 2008.

Reich, P. B.: The world-wide 'fast–slow' plant economics spectrum: a traits manifesto, J Ecol, 102, 275–301, https://doi.org/10.1111/1365-2745.12211, 2014.

Reichstein, M., Camps-Valls, G., Stevens, B., Jung, M., Denzler, J., Carvalhais, N., and Prabhat: Deep learning and process understanding for data-driven Earth system science, Nature, 566, 195–204, https://doi.org/10.1038/s41586-019-0912-1, 2019.

Rodrigues, M. and Riva, J. de la: An insight into machine-learning algorithms to model human-caused wildfire occurrence, Environ Modell Softw, 57, 192–201, https://doi.org/10.1016/j.envsoft.2014.03.003, 2014.

1209 Rouholahnejad, E., Abbaspour, K. C., Vejdani, M., Srinivasan, R., Schulin, R., and Lehmann,
1210 A.: A parallelization framework for calibration of hydrological models, Environ Modell Softw,
1211 31, 28–36, https://doi.org/10.1016/j.envsoft.2011.12.001, 2012.

1212 Sakschewski, B., Bloh, W., Boit, A., Rammig, A., Kattge, J., Poorter, L., Peñuelas, J., and
1213 Thonicke, K.: Leaf and stem economics spectra drive diversity of functional plant traits in a
1214 dynamic global vegetation model, Global Change Biol, 21, 2711–2725,
1215 https://doi.org/10.1111/gcb.12870, 2015.

1216 Sakschewski, B., Bloh, W. von, Boit, A., Poorter, L., Peña-Claros, M., Heinke, J., Joshi, J., and
1217 Thonicke, K.: Resilience of Amazon forests emerges from plant trait diversity, Nature Climate
1218 Change, 6, 1032–1036, https://doi.org/10.1038/nclimate3109, 2016.

1219 Sato, H., Itoh, A., and Kohyama, T.: SEIB–DGVM: A new Dynamic Global Vegetation Model
1220 using a spatially explicit individual-based approach, Ecol Model, 200, 279–307,
1221 https://doi.org/10.1016/j.ecolmodel.2006.09.006, 2007.

1222 Sawada, Y.: Machine Learning Accelerates Parameter Optimization and Uncertainty Assessment
1223 of a Land Surface Model, J Geophys Res Atmospheres, 125,
1224 https://doi.org/10.1029/2020jd032688, 2020.

1225 Sayad, Y. O., Mousannif, H., and Moatassime, H. A.: Predictive modeling of wildfires: A new
1226 dataset and machine learning approach, Fire Safety J, 104, 130–146,
1227 https://doi.org/10.1016/j.firesaf.2019.01.006, 2019.

1228 Shen, C.: A Transdisciplinary Review of Deep Learning Research and Its Relevance for Water
1229 Resources Scientists, Water Resour Res, 54, 8558–8593, https://doi.org/10.1029/2018wr022643,
1230 2018.

1231 Siefert, A., Violle, C., Chalmandrier, L., Albert, C. H., Taudiere, A., Fajardo, A., Aarssen, L. W.,
1232 Baraloto, C., Carlucci, M. B., Cianciaruso, M. V., Dantas, V. L., Bello, F., Duarte, L. D. S.,
1233 Fonseca, C. R., Freschet, G. T., Gaucherand, S., Gross, N., Hikosaka, K., Jackson, B., Jung, V.,
1234 Kamiyama, C., Katabuchi, M., Kembel, S. W., Kichenin, E., Kraft, N. J. B., Lagerström, A.,
1235 Bagousse-Pinguet, Y. L., Li, Y., Mason, N., Messier, J., Nakashizuka, T., Overton, J. McC.,
1236 Peltzer, D. A., Pérez-Ramos, I. M., Pillar, V. D., Prentice, H. C., Richardson, S., Sasaki, T.,
1237 Schamp, B. S., Schöb, C., Shipley, B., Sundqvist, M., Sykes, M. T., Vandewalle, M., and
1238 Wardle, D. A.: A global meta-analysis of the relative extent of intraspecific trait variation in
1239 plant communities, Ecol Lett, 18, 1406–1419, https://doi.org/10.1111/ele.12508, 2015.

1240 Sit, M., Demiray, B. Z., Xiang, Z., Ewing, G. J., Sermet, Y., and Demir, I.: A comprehensive
1241 review of deep learning applications in hydrology and water resources, Water Sci Technol, 82,
1242 2635–2670, https://doi.org/10.2166/wst.2020.369, 2020.

1243 Sitch, S., Smith, B., Prentice, I. C., Arneth, A., Bondeau, A., Cramer, W., Kaplan, J. O., Levis,
1244 S., Lucht, W., Sykes, M. T., Thonicke, K., and Venevsky, S.: Evaluation of ecosystem dynamics,
1245 plant geography and terrestrial carbon cycling in the LPJ dynamic global vegetation model: LPJ

DYNAMIC GLOBAL VEGETATION MODEL, Global Change Biol, 9, 161–185, https://doi.org/10.1046/j.1365-2486.2003.00569.x, 2003.

Snell, R. S., Huth, A., Nabel, J. E. M. S., Bocedi, G., Travis, J. M. J., Gravel, D., Bugmann, H., Gutiérrez, A. G., Hickler, T., Higgins, S. I., Reineking, B., Scherstjanoi, M., Zurbriggen, N., and Lischke, H.: Using dynamic vegetation models to simulate plant range shifts, Ecography, 37, 1184–1197, https://doi.org/10.1111/ecog.00580, 2014.

Snoek, J., Larochelle, H., and Adams, R. P.: Practical Bayesian Optimization of Machine Learning Algorithms, Arxiv, 2012.

Stark, S. C., Leitold, V., Wu, J. L., Hunter, M. O., Castilho, C. V. de, Costa, F. R. C., McMahon, S. M., Parker, G. G., Shimabukuro, M. T., Lefsky, M. A., Keller, M., Alves, L. F., Schietti, J., Shimabukuro, Y. E., Brandão, D. O., Woodcock, T. K., Higuchi, N., Camargo, P. B. de, Oliveira, R. C. de, Saleska, S. R., and Chave, J.: Amazon forest carbon dynamics predicted by profiles of canopy leaf area and light environment, Ecol Lett, 15, 1406–1414, https://doi.org/10.1111/j.1461-0248.2012.01864.x, 2012.

Strigul, N., Pristinski, D., Purves, D., Dushoff, J., and Pacala, S.: SCALING FROM TREES TO FORESTS: TRACTABLE MACROSCOPIC EQUATIONS FOR FOREST DYNAMICS, Ecol Monogr, 78, 523–545, https://doi.org/10.1890/08-0082.1, 2008.

Swenson, N. G. and Enquist, B. J.: Opposing assembly mechanisms in a Neotropical dry forest: implications for phylogenetic and functional community ecology, Ecology, 90, 2161–2170, https://doi.org/10.1890/08-1025.1, 2009.

Thakur, M. P. and Wright, A. J.: Environmental Filtering, Niche Construction, and Trait Variability: The Missing Discussion, Trends Ecol Evol, 32, 884–886, https://doi.org/10.1016/j.tree.2017.09.014, 2017.

Tsai, W.-P., Feng, D., Pan, M., Beck, H., Lawson, K., Yang, Y., Liu, J., and Shen, C.: From calibration to parameter learning: Harnessing the scaling effects of big data in geoscientific modeling, Nat Commun, 12, 5988, https://doi.org/10.1038/s41467-021-26107-z, 2021.

Uriarte, M., Swenson, N. G., Chazdon, R. L., Comita, L. S., Kress, W. J., Erickson, D., Forero-Montaña, J., Zimmerman, J. K., and Thompson, J.: Trait similarity, shared ancestry and the structure of neighbourhood interactions in a subtropical wet forest: implications for community assembly, Ecol Lett, 13, 1503–1514, https://doi.org/10.1111/j.1461-0248.2010.01541.x, 2010.

Violle, C., Enquist, B. J., McGill, B. J., Jiang, L., Albert, C. H., Hulshof, C., Jung, V., and Messier, J.: The return of the variance: intraspecific variability in community ecology, Trends Ecol Evol, 27, 244–252, https://doi.org/10.1016/j.tree.2011.11.014, 2012.

Wang, C., Duan, Q., Gong, W., Ye, A., Di, Z., and Miao, C.: An evaluation of adaptive surrogate modeling based optimization with two benchmark problems, Environ Modell Softw, 60, 167–179, https://doi.org/10.1016/j.envsoft.2014.05.026, 2014.

Wang, S. S. -C., Qian, Y., Leung, L. R., and Zhang, Y.: Identifying Key Drivers of Wildfires in the Contiguous US Using Machine Learning and Game Theory Interpretation, Earth's Futur, 9, e2020EF001910, https://doi.org/10.1029/2020ef001910, 2021.

Wang, S. S.-C., Qian, Y., Leung, L. R., and Zhang, Y.: Interpreting machine learning prediction of fire emissions and comparison with FireMIP process-based models, Atmos Chem Phys, 22, 3445–3468, https://doi.org/10.5194/acp-22-3445-2022, 2022.

Watson-Parris, D., Williams, A., Deaconu, L., and Stier, P.: Model calibration using ESEm v1.1.0 – an open, scalable Earth system emulator, Geosci Model Dev, 14, 7659–7672, https://doi.org/10.5194/gmd-14-7659-2021, 2021.

Weng, E. S., Malyshev, S., Lichstein, J. W., Farrior, C. E., Dybzinski, R., Zhang, T., Shevliakova, E., and Pacala, S. W.: Scaling from individual trees to forests in an Earth system modeling framework using a mathematically tractable model of height-structured competition, Biogeosciences, 12, 2655–2694, https://doi.org/10.5194/bg-12-2655-2015, 2015.

Wilson, K., Goldstein, A., Falge, E., Aubinet, M., Baldocchi, D., Berbigier, P., Bernhofer, C., Ceulemans, R., Dolman, H., Field, C., Grelle, A., Ibrom, A., Law, B. E., Kowalski, A., Meyers, T., Moncrieff, J., Monson, R., Oechel, W., Tenhunen, J., Valentini, R., and Verma, S.: Energy balance closure at FLUXNET sites, Agr Forest Meteorol, 113, 223–243, https://doi.org/10.1016/s0168-1923(02)00109-0, 2002.

Wright, I. J., Reich, P. B., Cornelissen, J. H. C., Falster, D. S., Garnier, E., Hikosaka, K., Lamont, B. B., Lee, W., Oleksyn, J., Osada, N., Poorter, H., Villar, R., Warton, D. I., and Westoby, M.: Assessing the generality of global leaf trait relationships, New Phytol, 166, 485–496, https://doi.org/10.1111/j.1469-8137.2005.01349.x, 2005.

Xu, T. and Liang, F.: Machine learning for hydrologic sciences: An introductory overview, Wiley Interdiscip Rev Water, 8, https://doi.org/10.1002/wat2.1533, 2021.

Zhang, J., Bras, R. L., Longo, M., and Scalley, T. H.: The impact of hurricane disturbances on a tropical forest: implementing a palm plant functional type and hurricane disturbance module in ED2-HuDi V1.0, Geosci Model Dev, 15, 5107–5126, https://doi.org/10.5194/gmd-15-5107-2022, 2022.

Zhang, Y., Ma, J., Liang, S., Li, X., and Li, M.: An Evaluation of Eight Machine Learning Regression Algorithms for Forest Aboveground Biomass Estimation from Multiple Satellite Data Products, Remote Sens-basel, 12, 4015, https://doi.org/10.3390/rs12244015, 2020.

Zheng, Z., Curtis, J. H., Yao, Y., Gasparik, J. T., Anantharaj, V. G., Zhao, L., West, M., and Riemer, N.: Estimating Submicron Aerosol Mixing State at the Global Scale With Machine Learning and Earth System Modeling, Earth Space Sci, 8, https://doi.org/10.1029/2020ea001500, 2021a.

Zheng, Z., Zhao, L., and Oleson, K. W.: Large model structural uncertainty in global projections of urban heat waves, Nat Commun, 12, 3736, https://doi.org/10.1038/s41467-021-24113-9, 2021b.

Zheng, Z., West, M., Zhao, L., Ma, P.-L., Liu, X., and Riemer, N.: Quantifying the structural uncertainty of the aerosol mixing state representation in a modal model, Atmos Chem Phys, 21, 17727–17741, https://doi.org/10.5194/acp-21-17727-2021, 2021c.

Zhu, Q., Li, F., Riley, W. J., Xu, L., Zhao, L., Yuan, K., Wu, H., Gong, J., and Randerson, J.: Building a machine learning surrogate model for wildfire activities within a global Earth system model, Geosci Model Dev, 15, 1899–1911, https://doi.org/10.5194/gmd-15-1899-2022, 2022.

Zuleta, D., Duque, A., Cardenas, D., Muller-Landau, H. C., and Davies, S. J.: Drought-induced mortality patterns and rapid biomass recovery in a terra firme forest in the Colombian Amazon, Ecology, 98, 2538–2546, https://doi.org/10.1002/ecy.1950, 2017.